NAVAL POSTGRADUATE SCHOOL
Monterey, California

THESIS

A STUDY OF THE MICROSTRUCTURAL BASIS FOR THE STRENGTH AND TOUGHNESS PROPERTIES OF WATER-QUENCHED AND AIR-COOLED HSLA-100, HSLA-100 WITH INCREASED COPPER, AND A ULCB STEEL

by

Thomas Campion Mohr

SEPTEMBER 1991

Thesis Advisor: Alan G. Fox

REPORT DOCUMENTATION PAGE

Form Approved
OMB No 0704-0188

1a. REPORT SECURITY CLASSIFICATION Unclassified	1b. RESTRICTIVE MARKINGS
2a. SECURITY CLASSIFICATION AUTHORITY	3. DISTRIBUTION/AVAILABILITY OF REPORT Approved for public release: Distribution is unlimited
2b. DECLASSIFICATION/DOWNGRADING SCHEDULE	
4. PERFORMING ORGANIZATION REPORT NUMBER(S)	5. MONITORING ORGANIZATION REPORT NUMBER(S)
6a. NAME OF PERFORMING ORGANIZATION Naval Postgraduate School 6b. OFFICE SYMBOL (If applicable) ME	7a. NAME OF MONITORING ORGANIZATION Naval Postgraduate School
6c. ADDRESS (City, State and ZIP Code) Monterey, CA 93943-5000	7b. ADDRESS (City, State, and ZIP Code) Monterey, CA 93943-5000
8a. NAME OF FUNDING SPONSORING ORGANIZATION 8b. OFFICE SYMBOL (If applicable)	9. PROCUREMENT INSTRUMENT IDENTIFICATION NUMBER
8c. ADDRESS (City, State, and ZIP Code)	10. SOURCE OF FUNDING NUMBER PROGRAM ELEMENT NO. / PROJECT NO. / TASK NO. / WORK UNIT ACCESSION NO

11. TITLE (Include Security Classification)
A STUDY OF THE MICROSTRUCTURAL BASIS FOR THE STRENGTH AND TOUGHNESS PROPERTIES OF WATER-QUENCHED AND AIR-COOLED HSLA-100, HSLA-100 WITH INCREASED COPPER, AND A ULCB STEEL

12. PERSONAL AUTHORS
THOMAS CAMPION MOHR

13a. TYPE OF REPORT	13b. TIME COVERED	14. DATE OF REPORT (Year, Month, Day)	15. PAGE COUNT
Master's Thesis	FROM ... TO ...	SEPTEMBER 1991	98

16. SUPPLEMENTARY NOTATION
The views expressed are those of the author and do not reflect the official policy or position of the Department of Defense or the U.S. Government

17. COSATI CODES			18. SUBJECT TERMS (Continue on reverse if necessary and identify by block numbers)
FIELD	GROUP	SUB-GROUP	HSLA, ULCB, non-metallic inclusions

19. ABSTRACT (Continue on reverse if necessary and identify by block numbers)

The microstructural basis for strength of the water-quenched and air-cooled HSLA-100, HSLA-100 with increased copper, and a ULCB steel was investigated by conducting an inclusion study and characterizing the microstructure of each of the steels. For the inclusion study, the SEM was used to examine a large number of fields and determine inclusion morphology while the EDX was used to determine inclusion composition. The microstructure of both the water-quenched and air-cooled steels was characterized using the optical microscope, SEM, and TEM.

The HSLA-100 with increased copper steel was adequately calcium treated and aluminum deoxidized as evidenced by the low sulfur content, few MnS stringers, and lack of large oxide arrays. The ULCB steel was not calcium treated or Al-killed; nor was it thermo-mechanically processed as shown by the lack of lipped, broken, or elongated stringers. Both MnS and oxide inclusions were present, and consequently, ladle metallurgy would have to be used before the ULCB steel was hot-worked.

(continued on next page)

20. DISTRIBUTION/AVAILABILITY OF ABSTRACT XX UNCLASSIFIED/UNLIMITED SAME AS RPT DTIC USERS	21. ABSTRACT SECURITY CLASSIFICATION unclassified	
22a. NAME OF RESPONSIBLE INDIVIDUAL Alan G. Fox	22b. TELEPHONE (Include Area Code) 408-646-2142	22c. OFFICE SYMBOL ME/Fo

continued from block 19

The microstructural basis for the strength of the as-quenched HSLA-100, HSLA-100 with increased copper, and ULCB steels is the transformation product packet size, small lath width, and high dislocation density. The as-quenched increased copper steel also contained ε-copper precipitates which added to its high level of strength and toughness. The as-quenched ULCB steel did not reach the desired strength level because its transformation product packet size was too large; approximately the same size as the prior-austenite grains. Thermo-mechanical processing of the steel would result in a finer packet size.

Air cooling of the HSLA-100 and HSLA-100 with increased copper steels introduced a significant amount of pro-eutectoid ferrite to their microstructures which would result in a lower level of strength. Air-cooling of the ULCB steel reduced the transformation product packet size by half. The finer packet size as a result of air cooling could alleviate the large expense incurred by water-quenching steel plate immediately following the final hot-rolling pass.

Approved for public release: Distribution is unlimited

A Study of the Microstructural Basis for the Strength and Toughness Properties of Water-Quenched and Air-Cooled HSLA-100, HSLA-100 With Increased Copper, and a ULCB Steel

by

Thomas Campion Mohr
Lieutenant, United States Navy
B.S., United States Naval Academy, 1985

Submitted in partial fulfillment of the requirements for the degree of

MASTER OF SCIENCE
IN MECHANICAL ENGINEERING

from the

NAVAL POSTGRADUATE SCHOOL

SEPTEMBER 1991

Author: Thomas Campion Mohr
Thomas Campion Mohr

Approved by: A. G. Fox
Alan G. Fox, Thesis Advisor

A.J. Healey, Chairman
Department of Mechanical Engineering

ABSTRACT

The microstructural basis for strength of the water-quenched and air-cooled HSLA-100, HSLA-100 with increased copper, and a ULCB steel was investigated by conducting an inclusion study and characterizing the microstructure of each of the steels. For the inclusion study, the SEM was used to examine a large number of fields and determine inclusion morphology while the EDX was used to determine inclusion composition. The microstructure of both the water-quenched and air-cooled steels was characterized using the optical microscope, SEM, and TEM.

The HSLA-100 with increased copper steel was adequately calcium treated and aluminum deoxidized as evidenced by the low sulfur content, few MnS stringers, and lack of large oxide arrays. The ULCB steel was not calcium treated or Al-killed; nor was it thermo-mechanically processed as shown by the lack of lipped, broken, or elongated stringers. Both MnS and oxide inclusions were present, and consequently, ladle metallurgy would have to be used before the ULCB steel was hot-worked.

The microstructural basis for the strength of the as-quenched HSLA-100, HSLA-100 with increased copper, and ULCB steels is the transformation product packet size, small lath width, and high dislocation density. The as-quenched increased copper steel also contained ε-copper precipitates which added to its high level of strength and toughness. The as-quenched ULCB steel did not reach the desired strength level because its transformation product packet size was too large; approximately the same size as the prior-austenite grains. Thermo-mechanical processing of the steel would result in a finer packet size.

Air cooling of the HSLA-100 and HSLA-100 with increased copper steels introduced a significant amount of pro-eutectoid ferrite to their microstructures which would result in a lower level of strength. Air-cooling of the ULCB steel reduced the transformation product packet size by half. The finer packet size as a result of air cooling could alleviate the large expense incurred by water-quenching steel plate immediately following the final hot-rolling pass.

TABLE OF CONTENTS

LIST OF TABLES

LIST OF FIGURES

I. INTRODUCTION

Modern warship design continues to increase its utilization of high strength, alloy steel plate for weight reduction, increased payload, and increased mobility. Naval ship structures are subjected to a complex spectrum of dynamic loadings and stresses from various sources such as fabrication and fit-up, wave loadings, sea slap, slamming, vibration, thermal excursions, cargo buoyancy, aircraft/helo landing, and weapons reactions. In addition, the ship structure must operate in both tropical and arctic seas over a temperature range of -30° to +120°F [Ref. 1:p. 1-2].

A second, but equally important requirement is that structural integrity be maintained in response to the effects of hostile weapons which submit the hull to loading in the form of severe shock waves. This requires the use of structural steels and welding materials which demonstrate high fracture toughness and flaw propagation tolerance [Ref. 1:p. 2]. Also, each of the above requirements must be met in an environment of severe fiscal constraint.

HY-80, HY-100, and HY-130 have traditionally been used in naval ship construction. However, the welding of the HY-series requires a number of fabrication controls to prevent post-weld cracking. These include preheat requirements, internal temperature limits, electrode preparation controls, heat input limits, storage and issue controls, weather protection, constraint

reduction, welder training and qualification, and an intensive inspection program; all of which dramatically increase the cost of production and reduce productivity. These increased costs resulted in the Navy initiating a High Strength Low Alloy research and development program with a goal of reducing shipbuilding costs. [Ref. 1:p. 2]

The HY series steels are martensitic in microstructure, and consequently, rely upon a quench and temper treatment and relatively high levels of carbon to attain the required strength and toughness. Unfortunately, these high carbon levels adversely affect the weldability of the material and result in the need for the fabrication controls discussed above. The newly developed HSLA-80 and HSLA-100 alloys have shown that alloy steels can have good strength and toughness without high carbon levels. The reduction in carbon requires an increase in strength through other alloying agents; the primary one used in the HSLA series being copper. Although the effectiveness of copper in increasing strength is much less than carbon there are fewer deleterious effects. The toughness of these alloys results from thermo-mechanical processing, microalloying, and improved steelmaking cleanliness [Ref. 2:pp. 26-27]. The use of HSLA steels has resulted in a significant reduction in hull fabrication costs, increased productivity due to reduced process controls and NDT requirements, and is currently used as the primary structural steel in the Ticonderoga class cruisers, Arleigh Burke class destroyers, and the Nimitz class aircraft carrier USS John C. Stennis [Ref. 1:p. 3].

Another approach to obtaining high strength, high toughness steels is the ultra-low-carbon bainitic (ULCB) alloys. In this system the carbon level is further reduced to 0.02-0.04% and alloying is used to control the bainitic shelf temperature (which in turn controls strength) while retarding ferrite formation. The toughness is dependent on the grain size which is manipulated by thermo mechanical processing and cooling rate. Recent research at the David Taylor Research Center and University of Pittsburgh has demonstrated that ULCB steels can be made with a strength of 80 to 140 ksi yield strength and satisfactory toughness. [Ref. 2:p. 27]

The Navy has a continuing HSLA steels research and development program to produce low cost alternatives to the HY series steel system. The development of a new 130 ksi yield strength grade will take advantage of new technologies such as low carbon bainite, microalloying, copper strengthening, and clean steelmaking, as well as more traditional metallurgy to provide an easily produced, inexpensive HSLA-130 grade steel. [Ref. 2:p. 27]

The object of this thesis is to investigate the microstructural basis for the strength and toughness properties of an HSLA-100 steel, which achieves the 100 ksi yield strength, an HSLA-100 steel with increased copper which achieves the 130 ksi yield strength level, and a ULCB steel with copper which does not reach the 130 ksi level.

II. BACKGROUND

A. THE DEVELOPMENT OF HSLA/ULCB STEELS

Historically, only one family of low alloy steel was able to exceed a yield strength of 690 MPa. This group of steels has a martensitic microstructure which requires a high carbon level for attaining the desired levels of strength, toughness, and hardenability (which is required for thicker sections of plate). While the base plate properties of a properly quenched and tempered martensitic steel meet design goals, the combination of relatively high carbon and alloy contents have rendered these steels difficult and expensive to fabricate, principally because of their poor welding characteristics. [Ref. 3:p. 45]

To meet this challenge, research in North America, Europe, and Japan concentrated on 1) developing an understanding of the factors affecting grain size, 2) development of a better understanding of the strengthening mechanisms involved in steel and the relations between the type of strengthening and its influence on the ductile to brittle transition temperature, 3) studying the effects of thermomechanical processing and composition and their influence on strength and toughness and 4) understanding the role of steel cleanliness with respect to toughness and developing methods for controlling cleanliness and inclusion morphology. [Ref. 4:p. 17]

The improved understanding resulting from such research has led to the continuing development of two different strong, tough, and weldable steels, the first being the High Strength Low Alloy (HSLA) series, and more recently the Ultra Low Carbon Bainitic steels (ULCB).

The steels combine carefully controlled heating and rolling procedures with optimum utilization of the microalloying additions niobium, vanadium, and titanium in low-carbon low-sulfur or sulfide-shape-controlled, high-cleanliness steels produced by special secondary steelmaking procedures, so that the steel may rely on strengthening mechanisms which are largely independent of carbon content, unlike the older heat treated ferrite-pearlite or martensitic plate steel [Ref. 4:p. 17] [Ref. 5:p. 317]. The various strengthening mechanisms include solution strengthening, dislocation strengthening, grain boundary strengthening, and particle dispersion strengthening which in combination make up for the loss of strength caused by the significantly reduced levels of carbon [Ref. 6:p. 26]. The two steels differ only in composition and the relative amount each strengthening mechanism is used to reach its target strength and toughness.

It cannot be overemphasized that this process of development was not haphazard, but was based on much systematic metallurgical research and can be regarded as a good example of how developments are based upon, and often wait upon, the understanding of structure-property relationships, transformations, etc. [Ref. 7:p. 62]

B. METALLURGICAL DESIGN OF HSLA-80, HSLA-100 STEELS

Nearly 50% of the total Department of Defense requirements for carbon, alloy, and steel plate is used in shipbuilding [Ref. 1:p. 1]. Consequently, the HSLA steel program was initiated to reduce shipbuilding costs to achieve an increased affordability in future warships, mainly by decreasing the required parameter controls when welding [Ref. 7:p. 2].

The impact of the low carbon content on weldability can best be seen on the Graville diagram, Figure 1, [Ref. 1:p. 16]. The Graville diagram uses the carbon and carbon equivalent (CE) content to establish three regions which predict the ease with which a steel can be welded. Carbon Equivalent is an indication of a material's ability to resist hydrogen-induced cracking during welding [Ref. 8:p. 22]. The traditional construction steels (HY-80, 100, and 130) lie in Region 3 which is difficult (and therefore expensive) to weld. Construction experience with this family of steels have given credence to this prediction. The HSLA family of steels have such a low carbon content that even with moderate to high carbon equivalent values, they fall into Zone 1 which predicts easily weldable steel. [Ref. 9:p. 6]

The Navy's HSLA development program identified and evaluated ASTM A710, Grade A steel as the prime candidate among a number of commercial HSLA steel plate products to replace its HY-80 steel in most applications [Ref. 1:p. 2]. ASTM A710 is a low carbon, copper precipitation strengthened steel with excellent weldability and toughness that can be welded without preheat

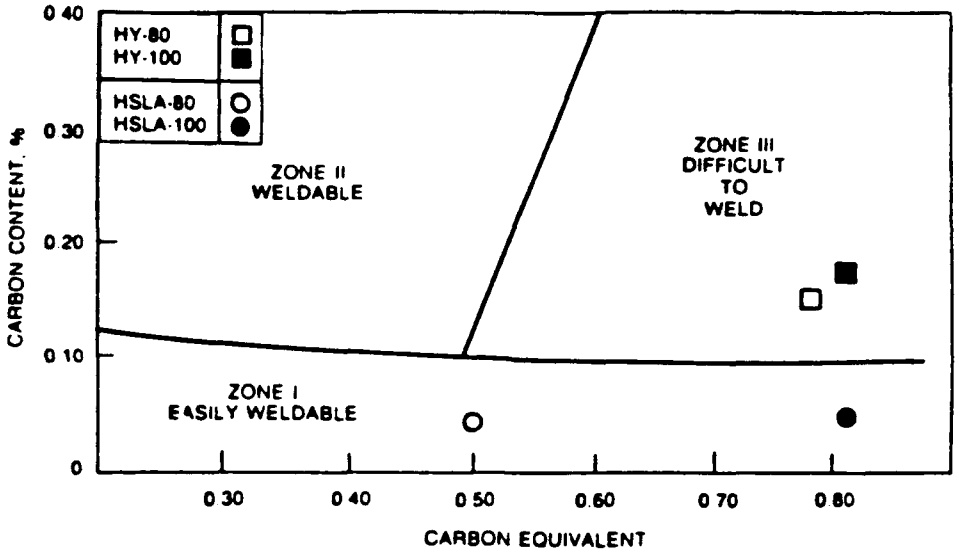

$$\left[CE = C + \frac{Mn + Si}{6} + \frac{Ni + Cu}{15} + \frac{Cr + Mo + V}{5} \right]$$

Figure 1. The Graville Diagram: Influence of Carbon Level and Carbon Equivalent on Susceptibility to HAZ Cracking of Steel Plate. [Ref. 10:p. 183]

in plate thicknesses up to 19mm (3/4 inch) [Ref. 11:p. 2]. In 1984, after an extensive evaluation of structural performance and mechanical properties, ASTM A710 was designated HSLA-80 (MiL-S-24645) and certified for use in ship construction.

Following the successful HSLA-80 program another alloy development program was undertaken to produce another highly weldable, copper precipitation strengthened steel at the 100 ksi (689.5 MPa) level. It was stipulated by the Navy that the new steel be copper precipitation strengthened, contain niobium for grain-size control, have maximum carbon, sulfur, and

phosphorous contents of 0.07%, 0.008%, and 0.010% respectively, and also contain at least the hardenability agents Mn, Ni, Cr, and Mo. It was also required that the steel be solution treated, quenched, and aged. The properties and weldability demonstrated by HSLA-100 steel resulted in certification of HSLA-100 (mil-S-2645A) in 1989. The composition range for HY-80, 100, and HSLA-80, and 100 as given by military specifications, is shown in Table I. [Ref. 11:p. 2] [Ref. 1:pp. 3-4]

TABLE I. CHEMICAL COMPOSITION OF HIGH STRENGTH STRUCTURAL STEELS. (MAJOR ELEMENTS FOR HEAVY GAGE PLATE, GREATER THAN 1 INCH) [Ref. 1:p. 4]

Element (weight %)	Specified Chemical Composition (maximum unless a range is shown)			
	HY-80 MIL-S-16216K	HSLA-80 MIL-24645A	HY-100 MIL-S-16216K	HSLA-100 MIL-S-24645A
C	0.13-0.118	0.06	0.14-0.20	0.06
Mn	0..10-0.40	0.40-0.70	0.10-0.40	0.75-1.05
P	0.015	0.020	0.015	0.020
S	0.008	0.006	0.008	0.006
Si	0.15-0.38	0.40	0.15-0.38	0.40
Ni	2.50-3.50	0.70-1.00	2.75-3.50	3.35-3.65
Cr	1.40-1.80	0.60-0.90	1.40-1.80	0.45-0.75
Mo	0.35-0.60	0.15-0.25	0.35-0.60	0.55-0.65
Cu	0.25	1.00-1.30	0.25	1.45-1.75
Nb	nil	0.02-0.06	nil	0.02-0.06

HSLA-80 and 100 steels achieve their strength through several mechanisms including grain refinement, precipitation strengthening, and solid solution strengthening. Another large contributor to the material's strength are dislocation substructures produced either by mechanical processing or by the bainitic/martensitic transformation which occurs throughout the material. Each of these strengthening mechanisms decrease dislocation mobility and accordingly, increase the stress required to move these dislocations. [Ref. 12:p. 6]

C. THE EFFECTS OF MICROALLOYING

Along with special thermo-mechanical processing techniques, the secret to the high strength and toughness of the HSLA and ULCB steel families is microalloying [Ref. 13:p. 41]. Alloy additions affect most strengthening mechanisms including grain size, precipitation and solid solution strengthening, and dislocation substructure development.

Dislocation substructure development is influenced by the addition of alloying elements by lowering the bainitic start and martensitic transformation temperatures which results in a still finer microstructure and a subsequent increase in strength. (See Figure 2)

Also of prime importance to microstructural development is the effect of alloying elements on the location of the proeutectoid ferrite C-curve. The shifting of the "C-curve" to the right allows the formation of bainite/martensite

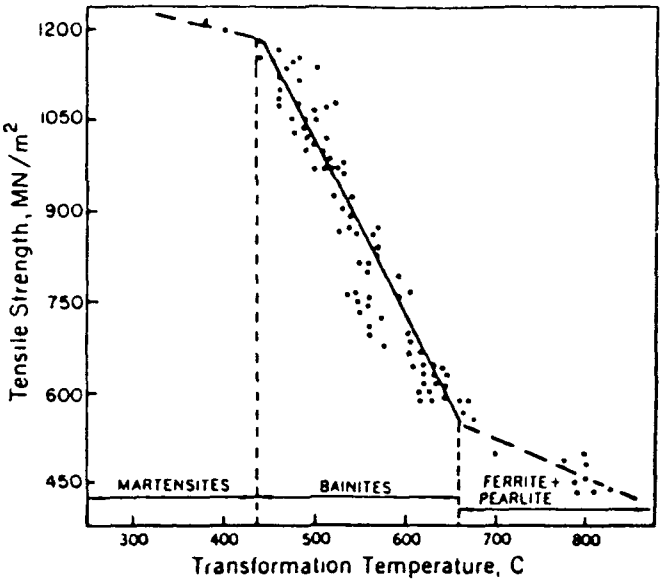

Figure 2. Effect of Transformation Temperature on the Strength of Ferrite-Pearlite and Bainitic Structures. [Ref. 14:p. 33]

with its corresponding fine microstructure and increased dislocation density, and also improves toughness because polygonal ferrite is deleterious to toughness in the through thickness direction. Figure 3 shows the effects of microalloying on the HSLA-80, A710 modified and HSLA-100 steels; note the resulting decrease in transformation temperature and movement of the C-curve to the right. The HSLA-100 steel used for this investigation has a carbon content of 0.048 wt% as compared to the carbon content of the steel used to develop the above HSLA-100 CCT diagram which was 0.06 wt%. The decrease in carbon content in the steel used reduces its hardenability by moving the "C-curve" further to the left than that shown by the above HSLA-100 CCT diagram. [Ref. 15:pp. 259-262.]

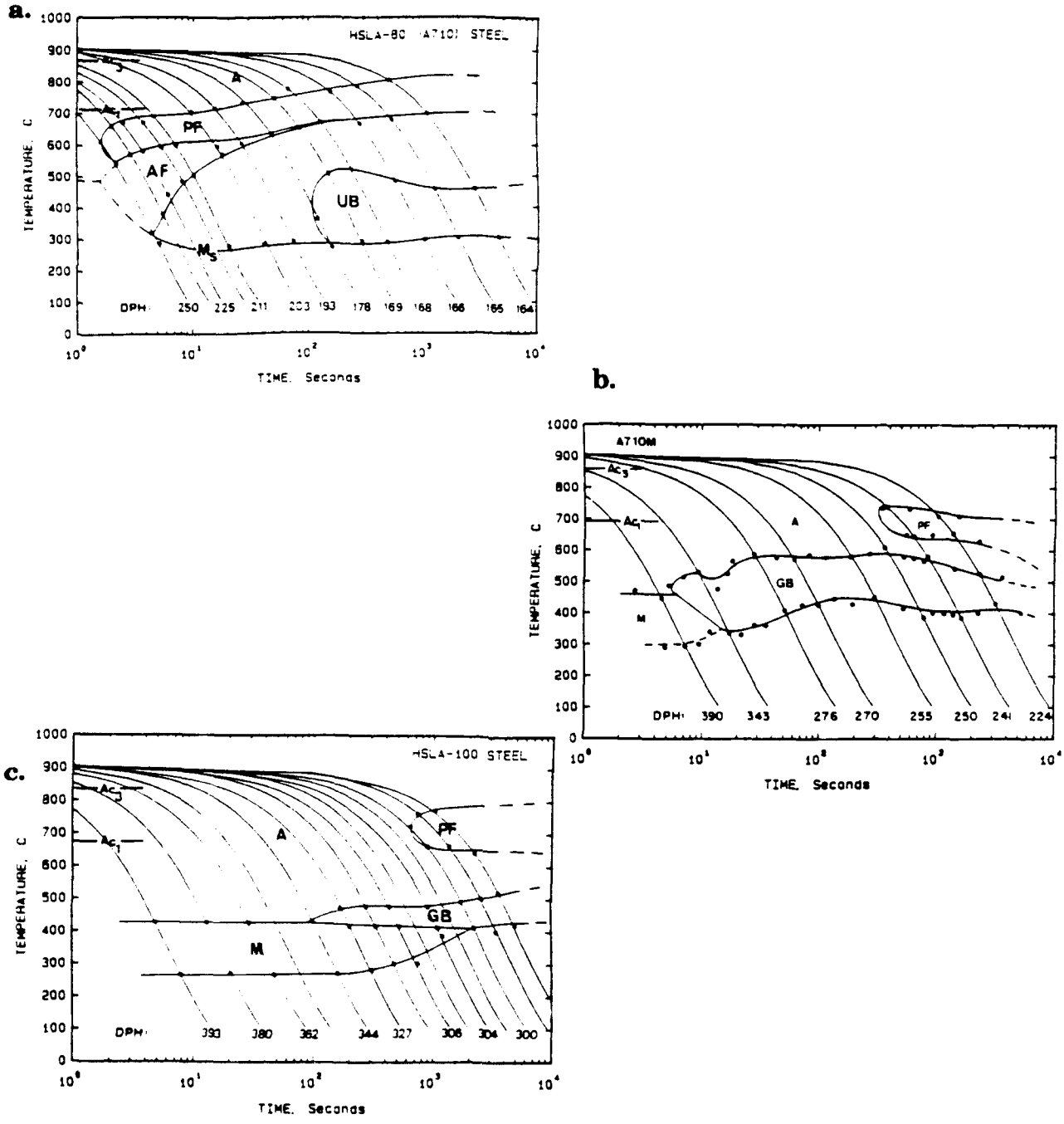

Figure 3. **a) Continuous Cooling Transformation (CCT) Diagram for HSLA-80; b) CCT Diagram for A710 Modified; c) CCT Diagram for HSLA-100; A=Austenite, PF=Proeutectoid Ferrite, AF=Acicular Ferrite, UB=Upper Bainite, MS=Martensite Start. [Ref. 16:p. 66]**

Listed below are the metallurgical significance of each of the major alloying elements. [Ref. 12:p. 8-9]

- **Carbon:** Increases hardenability by increasing a steel's ability to form martensite. Carbon is also a potent solid solution strengthener. Lower carbon content leads to improved toughness and a lower ductile to brittle transition temperature because fewer crack-initiating carbides exist. Low carbon concentrations also provide a highly weldable steel insensitive to hydrogen-induced cracking (HIC), and consequently, the need for pre-heat can be eliminated. [Ref. 16:pp. 64-65]

- **Manganese:** Combines with sulfur to form MnS, which precludes "hot cracking" caused by the formation of FeS films at grain boundaries; excellent deoxidizer; hardenability agent. [Ref. 17:p. 376.]

- **Copper:** Increases strength and toughness by precipitation of copper particles during aging; improves corrosion resistance to seawater, and hardenability. [Ref. 15:p. 260]

- **Nickel:** Extremely potent toughening agent; lowers DBTT; hardenability agent; austenite stabilizer. [Ref. 17:p. 376]

- **Niobium:** Combines with nitrogen and carbon to form niobium carbonitrides Nb(C,N) which provide grain refinement during hot-rolling and later re-austenizing treatment by pinning grain boundaries. [Ref. 15:p. 260]

- **Molybdenum:** Hardenability agent in quenched and tempered steels; suppresses temper embrittlement; solid solution strengthener; strong carbide former. [Ref. 17:p. 376]

- **Vanadium:** Strong carbide and nitride former. [Ref. 17:p. 376]

- **Silicon:** Strong deoxidizer; increases yield strength and DBTT when found in solid solution. [Ref. 17:p. 376]

- **Chromium:** Provides corrosion resistance; hardenability agent; solid solution strengthener, and strong carbide former. [Ref. 15:p. 376]]

- **Aluminum:** Strong deoxidizer; forms AlN, which pins grain boundaries and keeps ferrite grain size small. AlN formation also serves to remove N from solid solution, thereby lowering the DBTT. [Ref. 15:p. 376]

As previously stated, the addition of copper aids in the reduction of the deleterious effects of hydrogen-induced cracking. This phenomenon begins with hydrogen entering the steel from various sources such as a certain welding operations or wet corrosion in a wet hydrogen-sulfide containing environment. The hydrogen then diffuses to the inner surfaces of voids and cracks where the pressure can be raised dramatically to as much as several thousand atmospheres. Cracks then initiate chiefly at MnS colonies and propagate approximately to the size of each colony. Interconnection of adjacent parallel cracks may occur in a stepwise manner through the thickness as shown in Figure 4, depending on the size and distribution of the colonies and the existence of tensile stresses. Copper addition aids in the reduction of hydrogen induced cracking by preventing hydrogen entry into the steel by the formation of a protective film at grain boundaries. Consequently, copper treated steels show a reduction in average crack length with increasing weight percent copper (Figure 5). [Ref. 18:pp. 118-120]

D. STRUCTURE-PROPERTY RELATIONSHIPS IN BAINITIC STEELS

Bainitic microstructures can arise in commercial steels by appropriate design of the alloy composition, by suitable control of processing, or as a result of fabrication conditions, and currently represents the frontiers of research in

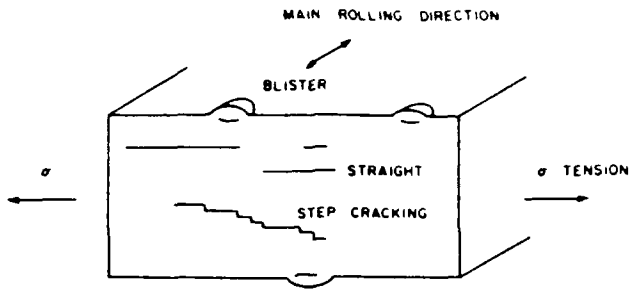

Figure 4. **Schematic Illustration of Hydrogen Induced Cracking in a Transverse Section. [Ref. 18:p. 119]**

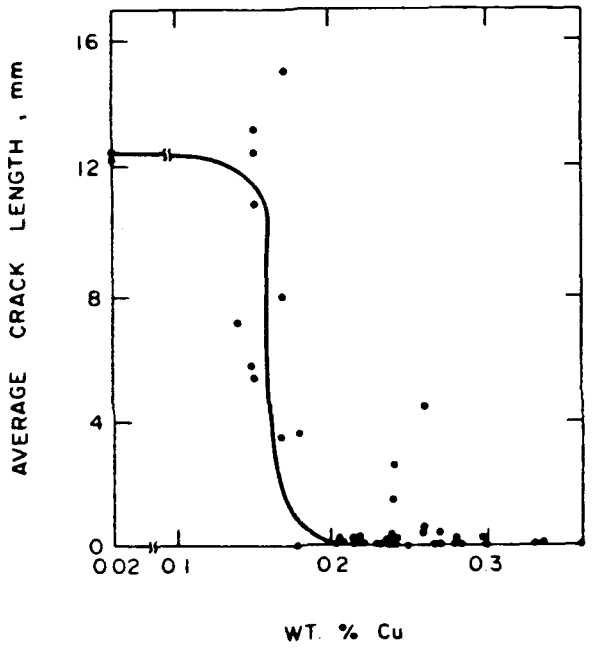

Figure 5. **Effect of Copper on the Average Crack Length. [Ref. 18:p. 120]**

the science of phase transformations. However, the significance of bainite as a transformation product lies in its positive effect on mechanical properties and

the extent to which these positive effects can be exploited by the design and heat treatment of commercial steels. [Ref. 19:p. 1527]

Bainite is a two phase microstructure consisting of carbide particles dispersed in a ferrite matrix and has two distinct morphologies depending upon the transformation temperature [Ref. 20]. The austenite-bainite decomposition involves first a martensitic shear transformation followed by a diffusion of carbon atoms which precipitate out as carbides [Ref. 21:p. 430]. The first formed nucleus is generally considered to be ferrite [Ref. 14:p. 110].

As mentioned above, bainite has two distinctly different morphologies depending upon the temperature at which their transformation occurs. "Upper Bainite" occurs as temperatures above 350°C in steels with greater than 0.6% carbon, but at somewhat higher temperatures in lower carbon steels. At these temperatures, carbon is sufficiently mobile to diffuse to the austenite in front of the growing ferrite. Therefore, carbon enriched austenite is entrapped between bainitic ferrite laths and may be retained, form martensite, or Fe_3C between laths depending upon the amount of carbon present and the rate of transformation. If the structure contains retained austenite or martensite it is referred to as "granular bainite." The general morphology is one of long laths with elongated particles or films lying between the laths. The lower the transformation temperature, the finer are the bainitic laths. The higher the

carbon content, the finer are the bainitic laths and the more numerous and continuous are the carbide films between the laths. [Ref. 14:pp. 110-111]

"Lower bainite" is the second of the bainitic morphologies and occurs at lower transformation temperatures. Because of the lower transformation temperatures the carbon cannot readily diffuse away from the growing ferrite and the initial ferrite plates are supersaturated with carbon. To maintain the driving force for this reaction the carbon precipitates within the ferrite laths as carbide plates at a characteristic angle of 55° to the long axis of the lath [Ref. 14:p. 111]. The characteristics of the ferrite in lower bainite, particularly in higher carbon steels is different from that of upper bainite in that the ferrite grains are often platelike [Ref. 19:p. 1528]. The lower the transformation temperature or the higher the carbon content, the finer the laths/plates, and the finer and more numerous the carbide particles [Ref. 14:p. 111].

Upper and lower bainite are terms most often applied to relatively higher carbon steels. Low carbon HSLA/ULCB steels rely upon a different type of austenite transformation product referred to as "acicular ferrite." Acicular ferrite has many morphological similarities to bainite (it is comprised of lath-like ferrite grains with a high dislocation density), and forms by the same diffusion-controlled shear mechanism. The crucial difference between the two is the very low carbon content of the acicular ferrite, which effectively removes any intra-lath carbides and yields much improved toughness. [Ref. 22:p. 13]

In upper and lower bainite, and acicular ferrite, low angle boundaries exist between ferrite laths/plates, which are obstacles to dislocation movement, but not for crack propagation. High angle boundaries exist between packets and prior austenite grain boundaries, which impede both dislocations and propagating cracks. [Ref. 14:p. 111]

It is possible to account for the strength of bainitic steels with four major mechanisms: [Ref. 19:pp. 1530-1532]

- **Lath strengthening:** There have been a number of studies which have attempted to find the relationship between strength and transformation product dimensions, but with varying results. However, most agree that flow stress varies with the reciprocal of some lath dimension such as lath length, width or colony/packet size.

- **Dislocation density:** Qualitative experiments using the TEM have shown that bainite has a "high" dislocation density, although very little quantitative analysis has been done to support this. It has been estimated that a dislocation density of 10^{14} m^{-2} raises the strength by approximately 145 Nmm^{-2}, and that the dislocation density increases as the transformation temperature is reduced. [Ref. 23:p. 773]

- **Interstitial and substitutional atom strengthening:** Evidence exists that there is a higher than equilibrium concentration of carbon atoms bound to dislocations in bainitic ferrite which make a significant contribution to strength; approximately 150 to 200 Nmm^{-2}. For substitutional elements, there is normally not enough time during the transformation to allow for their repartitioning, and their contribution to strength is well documented.

- **Carbide strengthening:** Carbide particles formed at lath boundaries in upper bainite appear to impede dislocation motion, thereby confining slip within the laths and increasing strength. A similar affect occurs in lower bainite.

Bainite has also been shown to have excellent toughness properties. Most studies agree that the major structural unit which characterizes this is the cleavage facet size. The cleavage facet size has been found to be slightly larger than the bainite packet size which suggests that crack deflection occurs at bainite/martensite colony boundaries as shown by Figures 6a and b. [Ref. 19:p. 1533]

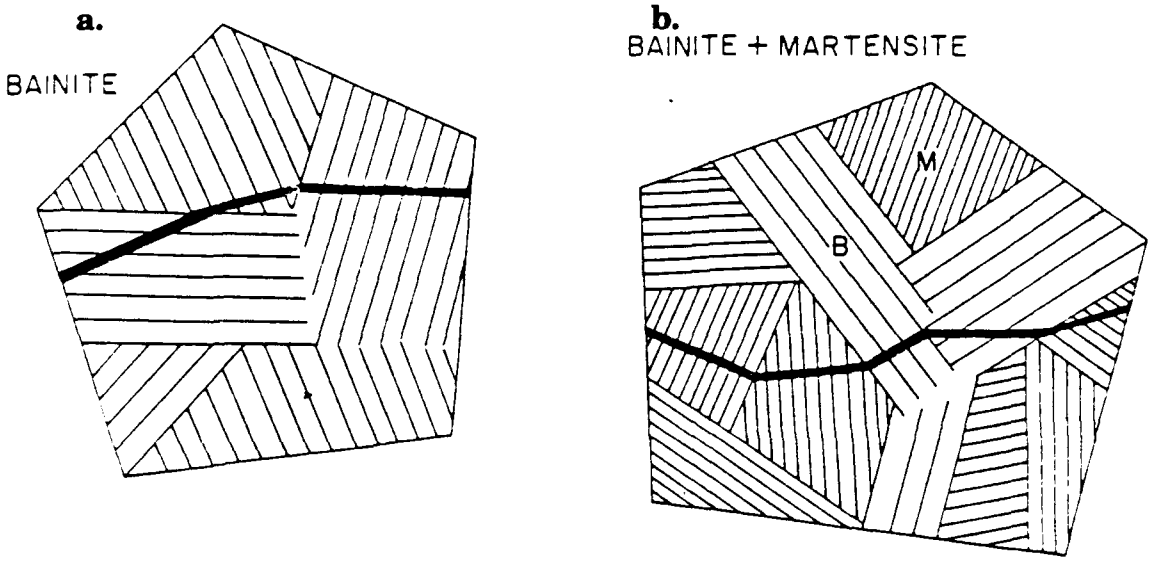

Figure 6. Cleavage Crack Deflection at: a) Bainite Packet Boundaries, b) Bainite and Lath Martensite Boundaries. [Ref. 19:p. 1533]

Upper bainite in low carbon steels has inferior impact resistance compared with lower bainite. The reasons for this behavior are: a) in upper bainite, large carbides will form supercritical crack defects, and once initiated the crack will only be deflected by high angle packet boundaries or prior austenite grain boundaries; b) in lower bainite, the smaller carbides are not

large enough to form supercritical defects and thus cracks are not easily initiated. Once a crack is started, however, its propagation is halted by the many carbides and increased dislocation density. [Ref. 14:p. 116]

There are two methods for raising the toughness of bainitic steels. First, processing the steel either by microalloying additions or thermo-mechanical treatment to reduce the prior-austenite grain size which will both increase toughness and lower the DBTT. And second, by promoting a subdivision of the parent austenite by, for example, multiple bainite/martensite packets. [Ref. 19:p. 1533].

E. THERMO-MECHANICAL TREATMENT OF HSLA/ULCB STEELS

The purpose of the thermo-mechanical treatment of steels is to take advantage of the effect of plastic deformations on the micro-structure of austenite in such a way as to develop the most favorable microstructure upon transformation [Ref. 24:p. 1703]. For HSLA/ULCB steels the most favorable microstructure is a small as possible ferritic packet size which provides a favorable balance of strength and toughness in the as-rolled steels. [Ref. 25:p. 61]

The first stage in the process is slab reheating during which certain microalloying additions such as Niobium, vanadium, or titanium dissolve and perform the following functions: [Ref. 24:p. 170] [Ref. 25:p. 62]

- maintain the fine austenite grain size during reheating by increasing the grain coarsening temperature;
- retard or suppress recrystallization;
- slow down the growth of recrystallized grains upon precipitation as carbides and nitrides by pinning grain boundaries.

The temperature at which the slab reheating is accomplished must be carefully chosen because a balance must be struck between the need to maximize the dissolution of the microalloy carbonitrides and the need to limit austenite grain growth. A fine, as re-heated, austenitic grain size results in the smallest possible ferritic packet size after transformation. [Ref. 25:pp. 62-63]

The rolling process is the next step in the thermo-mechanical treatment. During this process substructural features in the deformed (and recrystallized) austenite provide nucleation sites for microalloy carbonitrides precipitation. The precipitates themselves tend to pin the substructure, and consequently, inhibit recrystallization [Ref. 25:p. 64]. These interactions enable the rolling passes to be made at a temperature below the material's recrystallization temperature thereby ensuring the plastically deformed austenitic grains remain flattened [Ref. 25:p. 64]. The resulting high ratio of austenitic grain boundary surface area to grain volume increases the number of ferrite nucleation sites and aids significantly in obtaining a fine transformation product packet size upon cooling as shown in Figure 7. [Ref. 26:p. 25]

Figure 7. Relationship Between Austenitic Grain Thickness and Ferritic Grain Size Formed on Subsequent Transformation. (T_r=Temp. of Recrystallization) [Ref. 25:p. 65]

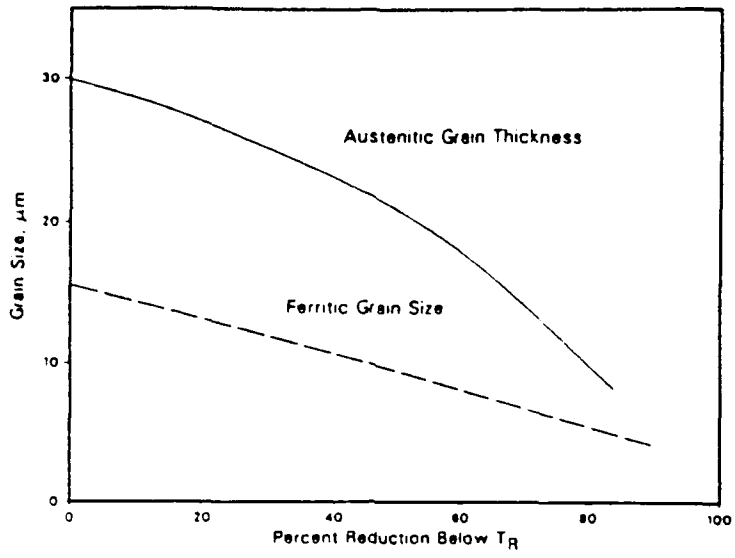

The transformation of the conditioned austenite into ferrite is the next step in the TMP and determines the final ferrite grain size and associated mechanical properties. Ferrite packets are nucleated at austenitic grain boundaries and deformation twins; overall, the mean ferritic grain size is related to the thickness of the flattened austenitic grains as also shown in Figure 7. Even after the minimum austenitic grain size is obtained the temperature range of the austenite-ferrite transformation must be controlled so that ferrite nucleation can be maximized and growth minimized. This is normally achieved by alloying or rapid cooling. [Ref. 25:p. 66]

Although a fine grain size delivers the best combination of strength and toughness there is a practical limit to the yield strength level which can be obtained (about 450 MPa for a grain size of 3 microns). For higher strength levels additional strengthening mechanisms must be used which may have a deleterious effect on toughness. Further strengthening can be obtained by making any number of final rolling passes, at progressively lower temperatures. This last TMP results in a warm worked ferritic structure and the desired level of strength, but unfortunately, at correspondingly lower levels of toughness. [Ref. 25:pp. 66-67]

F. THE ROLE OF INCLUSIONS

HSLA and ULCB steels, like any other steel, are actually a composite material composed of a metallic matrix and various second phase particles which can be both metallic and non-metallic in composition [Ref. 12:p. 22]. Early investigations of these non-metallic second phase particles, or "inclusions," thought of them merely as "dirt" or a "disease" which were always harmful to a steel, and consequently it was felt that they must always be kept to a minimum. This earlier characterization is now being changed, for while it is true that large exogenous inclusions are usually deleterious and should be avoided, this is only one aspect of the subject. There are approximately 10^{12}-10^{13} inclusions present in every ton of steel and their presence is sometimes harmful, but other times advantageous. Whatever their effect, they are an

inseparable part of the steel "matrix" and must be used to advantage in the final product. [Ref. 27:part 1, pp. i-ii].

1. Sources of Inclusions

Non-metallic inclusions fall into two groups, those of indigenous and those of exogenous origin. Indigenous inclusions occur as a result of reactions taking place in the solidifying steel bath, whereas exogenous inclusions result from the mechanical incorporation of slags, refractories, or other materials with which the molten steel comes in contact. Indigenous inclusions are formed by reactions induced either by additions to the steel or by changes in solubility during the cooling of the steel and are composed principally of oxides and sulfides. Exogenous inclusions are characterized by a generally larger size, sporadic occurrence, preferred location in the ingot or casting, irregular shapes and complex structure. They are mostly composed of oxides, a result of the composition of most slags and refractories. A small list of possible inclusion sources is given in Table II. [Ref. 27:part 3, p. 1]

The division of inclusions into two separate groups is a good starting point for this topic, but must be understood as an oversimplification. Indigenous precipitation often occurs on exogenous nuclei during the different stages of the steelmaking process. And also, an indigenous inclusion, its origin from either homogenous nucleation or from an exogenous fragment, will continuously change its composition in the molten steel bath, and even in the solid steel, until a time when the diffusion rate is almost negligible. The

TABLE II. POSSIBLE INCLUSION SOURCES AND KEY ELEMENTS
[Ref. 27:part 3, p. 3]

Possible inclusion Sources		Key Elements
Furnace	Furnace slags Furnace refractories Ferroalloys	Ca Ca Cr, Al, Si
Tapping	Launder refractories Oxidation	Mg, Ti, K FeO
Ladle	Deoxidation Ladle slag Ladle refractories	 Ca, Mg Mg, Ti, K
Teeming	Stopper and nozzle refractories Oxidation Deoxidation	Mg, Ti, K FeO
Ingot mold	Refractories Deoxidation	Mg, Ti, K
Heat treatment and rolling	Surface oxidation Surface sulfurizatino Inner oxidation Hot-shortness	FeO FeS SiO_2 FeS
Welding	Welding slags Electrode coatings Steel inclusions Hot tearing	Ca, Ti Ti, V S

metallographer therefore has a much harder time identifying the origin of most inclusions than the general classification suggests. [Ref. 27:part 3, p. 2]

2. Composition of Inclusions in Steel

The composition of inclusions falls into two broad categories; oxides and sulfides. The oxide group is dominated by the system $MnO\text{-}SiO_2\text{-}Al_2O_3$ in

silicon-manganese killed steels. This is the main system to which most other indigenous inclusions are related [Ref. 27:part 2, p. 1] [Ref. 12:p. 24]. Other common systems are $MgO\text{-}SiO_2\text{-}Al_2O_3$ and $CaO\text{-}SiO_2\text{-}Al_2O_3$, but they are formed mostly from exogenous nuclei. Calcium aluminate inclusions ($XCaO\text{-}YAl_2O_3$) are abundant in aluminum killed and calcium treated steels [Ref. 12:p. 24]. These inclusions are comparatively hard and often keep their spherical shape, even after working the steel. However, if the steel is more heavily deformed, especially at higher temperatures, they can break up into undesired stringers [Ref. 27:part 2, p. 45].

Sulfur base inclusions form the second largest category. Sulfur is soluble in the molten steel phase, but its solubility in the solid steel phase is very low. It precipitates in the form of metal sulfides during the solidification process; most commonly in the form of MnS [Ref. 27:part 2, p. 97]. MnS deforms upon hot working into large stringers causing anisotropic mechanical properties. However, in calcium or rare earth treated steels containing less than about 0.005 wt%S, the formation of MnS is precluded by the formation of inclusions such as CaS and CeS which are much less susceptible to deformation [Ref. 28:p. 1].

3. The Effects of Inclusions on Steel Properties

The ultimate purpose of the study of inclusions is to obtain a steel with improved properties. As a rule, exogenous inclusions should be avoided. For indigenous inclusions the problem is much more complicated because they

are a natural component of the steel. And even though their quantity, shape, size, distribution, and composition can be modified, they can never be completely avoided. Fortunately, these same properties have been shown to have a large impact on important steel parameters, and if properly manipulated, can result in a steel with the desired level of fracture toughness, ductility, machinability and fatigue resistance. [Ref. 27:part 3, p. 74]

A common problem in HSLA/ULCB steels is a lack of ductility which leads to lamellar tearing in plates during or after welding, or poor impact toughness in the through-thickness direction in plates. Generally, ductility decreases exponentially as the volume fraction of non-metallic inclusions increases (Figure 8). The major cause of this is when inclusions, particularly sulfides, are elongated into stringers during the hot-rolling process. This effect is magnified with very deformable particles, and, while this is true of manganese sulfides, oxides can also behave in this manner. [Ref. 14:pp. 83-84]

Ductile fracture in steels is caused by the nucleation, growth, and coalescence of voids which originate at hard particles such as inclusions. Inclusions are harder than the surrounding matrix which leads to stress concentrations during matrix deformation that will form voids by matrix-particle decohesion or by fracture of the particles. Voids form more easily if the particle is rigid, has a low cohesion to the matrix, or has a low internal fracture strength. Consequently, voids form more easily at large MnS inclusions than at smaller oxide inclusions. The voids grow until sudden strain

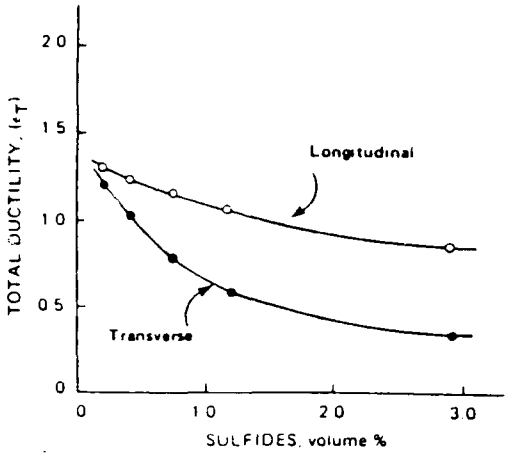

Figure 8. Effect of Sulfide Volume Fraction on Longitudinal and Transverse Total Ductility at Fracture. [Ref. 14:p. 82]

localization leads to failure. For a given matrix and inclusion type there is a minimum particle diameter below which voids will not grow; for most cases, approximately 1 micron [Ref. 29:p. 145]. Inclusions significantly decrease the Charpy impact shelf energy above the transition temperature, particularly in the through-thickness direction in plates (see Figure 9) [Ref. 15:p. 83]. The anisotropy of the notch toughness in plate steels is tied to the anisotropy in the shape of the inclusions and is more pronounced for manganese sulfides and those oxides which are deformed into stringers [Ref. 27:part 3, p. 103].

Inclusions can also be detrimental to fatigue properties if they are above a critical size and are relatively brittle at the temperature of loading. Dangerous inclusions include single phase Al_2O_3, spinels, and calcium-luminates with a size above 10 microns, and relatively less harmful are

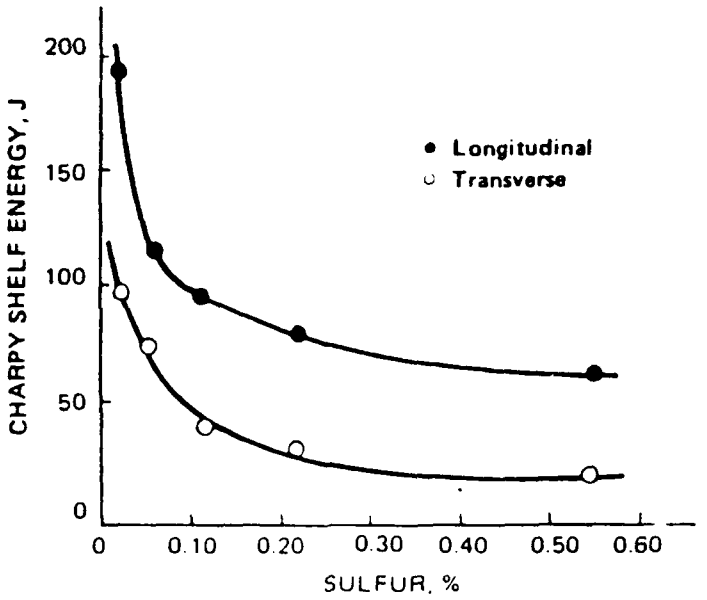

Figure 9. Effect of Sulfur Content (Sulfide Volume Fraction) on Longitudinal and Transverse Charpy Shelf Energy Value. [Ref. 14:p. 84]

sulfides. In the high cycle range, > 10^5 Hz, all cracks originate at inclusions. [Ref. 29:pp. 134-135]

Elongated sulfide and oxide stringers can cause lamellar tearing in rolled steel plate in areas where welding has imposed large through- thickness stresses by restraint of the structure if the long axis of the inclusions are perpendicular to the stress. These cracks occur just outside the transformed heat-affected zone, have a characteristic stepped appearance, and can lead to the failure of the joint. [Ref. 29:pp. 109-110]

The above deleterious effects of particular inclusions on mechanical properties can be significantly reduced and in some cases eliminated using

ladle metallurgy (also called secondary steelmaking) [Ref. 12:p. 28]. Ladle metallurgy involves the use of the ladle not only to transfer molten steel from the melting furnace to the continuous casting machine or ingot mold, but also as a vessel in which further refining operations can be performed. These refining operations, most of which have been developed in the past 20 years, enable precise control of inclusion number, size, composition, and morphology. [Ref. 29:p. 44]

Minimizing oxide inclusions, with a benefit to formability, weldability, and toughness can be accomplished with vacuum technology, bath electromagnetic stirring, and the addition of aluminum (Al killing) and calcium. The minimization of anisotropy in toughness and ductility by sulfide inclusion shape control is obtained from the use of zirconium, titanium, or calcium; calcium providing the additional benefits of being a desulfurizing agent and which also modifies deleterious Al_2O_3 inclusions into strong, hard calcium aluminates. Many of the mechanisms by which these inclusion modifications work still require to be resolved. Despite this, these metallurgical advances have significantly contributed to the current sophisticated HSLA/ULCB steel production, processing, and use. [Ref. 22:p. 27]

G. SCOPE OF PRESENT WORK

The replacement of the HY family of steels with the equivalent-strength HSLA series is being vigorously pursued by the U.S. Navy. Previous work on

HSLA-100 has been concerned with the verification of mechanical and welding properties and the examination of the microstructure at various aging temperatures. It is generally agreed that HSLA-100 has a microstructure comprised mostly of lath martensite with some acicular ferrite together with small amounts of interlath retained austenite in the as-water-quenched condition. The strength and toughness of this as-quenched steel finds its basis in the fine grained martensitic/bainitic microstructure resulting from the transformation of the warm worked "pancaked" fine prior austenite microstructure.

For this study information regarding the composition, size, and distribution of non-metallic inclusions and data concerning the lath martensite/ acicular ferrite microstructure of a ULCB and a high copper HSLA-100 steel in the as-water quenched and air-cooled condition has been collected. The purpose of this thesis is to study the microstructural basis for the strength and toughness of these two steels in the two different cooling conditions.

III. EXPERIMENTAL PROCEDURE

A. MATERIAL

David Taylor Research Center (DTRC) of Annapolis, Maryland, provided the following: one as-quenched HSLA-100 Charpy half, one as-quenched HSLA-100 with increased copper Charpy half, and a 40 mm x 30 mm x 27 mm section of air-cooled ULCB steel plate. The HSLA-100 sample was from the Lukens Steel Company. The exact processing information was reported previously by Mattes [Ref. 9:p. 26]. The HSLA-100 with increased copper was from the Phoenix Steel Company. Melts were formed in a 150-ton electric arc furnace, argon injected with CaSi, cast into ingots and slabbed for rolling to 3/4 inch. The as received steel plate was austenized for one hour at 1650°F and water quenched after which the Charpy samples were cut from the T-L directions [Ref. 30]. And lastly, the ULCB sample was from the Basic Metals Processing Research Institute, University of Pittsburgh; the exact processing information was restricted due to proprietary concerns.

The air-cooled ULCB was re-austenized at 950°C for one hour and water quenched. Later, approximately a 10 mm cube of each sample (HSLA-100, HSLA-100 with increased copper, and ULCB) was partitioned, re-austenized at 900°C for one hour and air-cooled. The result was both an air-cooled and water quenched portion of each sample available for microscopy.

Table III provides the chemical compositions and grain size of each of the steels as determined by DTRC.

TABLE III. HSLA-100, HSLA-100 WITH INCREASED COPPER, AND ULCB STEEL CHEMICAL COMPOSITION AND GRAIN SIZE

	C	Mn	Si	P	Cr	Ni	Al	S	Mo	Cu	Nb	Ti	N	O
HSLA-100 with increased copper	.047	.85	.22	.010	.57	3.59	.021	.005	.60	2.0	.025	--	--	--
HSLA-100	.048	.69	.27	.010	.52	3.42	--	.0004	.0091	1.47	.02	--	.0091	.0035
ULCB	.02	1.93	.33	.007	1.35	3.0	.023	.006	.97	1.35	.044	.014	.006	.002

	Grain Size (um)
HSLA-100 with increased copper	15
HSLA-100	*
ULCB	14

* Similar to HSLA-100 because of similar microstructures in the as-quenched condition.

B. MECHANICAL PROPERTIES

Charpy V-notch impact energy, yield strength, ultimate tensile strength, and ductility testing of each steel was conducted by DTRC and the data provided to the author. SEM and TEM micrographs taken by the author were used to measure the dimensions of the bainite packets. Specifically, packet size was determined from secondary electron, etched SEM photos employing a mean intercept method. The length of the bainite laths were measured from the same micrographs and averaged, and bainite lath widths were measured

from TEM micrographs (due to their small size) using a mean intercept method.

C. MICROSCOPY

1. Optical Microscopy

Optical microscopy was conducted to photograph inclusions and analyze the etched microstructure. The samples were mounted and ground with successive emery paper to 600 grit and polished using 6 micron and 1 micron diamond paste. The specimen was washed with soap, rinsed with water, followed by a rinse in ethanol and blown dry between polishing media. Extreme care was taken to maintain cleanliness since retained polishing media can contaminate the diamond wheels, resulting in erroneous EDX analysis and poor surface finishes.

The unetched specimen was then placed in a Zeiss ICM 405 photomicroscope and examined. Various magnifications were used to photograph a variety of inclusions. The mounted sample was then etched for approximately 30 seconds, using a two percent nital etching solution. The exposed microstructure was then again examined and photographed at several magnifications.

2. Scanning Electron Microscopy

Using the unetched samples, a Cambridge Stereo Scan S200 Scanning Electron Microscope and a Kevex 8000 Energy Dispersive X-Ray

Analysis (EDX) were used to perform an inclusion study consisting of 300 random fields for the HSLA sample and 150 random fields for the ULCB sample both at 1000X magnification. A chemical analysis was performed using the EDX on each observed inclusion which provided information on the inclusion's chemical composition. Spectra for each inclusion were collected and analyzed. Photographs of several inclusions using back scatter and secondary electron images were taken.

Using the etched samples, microstructural features such as bainite packet size and lath length were examined and photographed at various magnifications and measured from photographs taken at 1500X.

3. Transmission Electron Microscopy

Thin wafers from the HSLA and ULCB samples were cut using the low speed diamond wafer saw. Discs 3 mm in diameter were then punched out and mechanically thinned on wet 600 grit silicon carbide paper to a thickness of less then .025 mm. Discs were electrochemically thinned to perforation in a Struers Tenupol electropolishing device, operating at 70 volts, 0.5 Amperes, and a medium flow rate using either a solution of 3% perchloric acid, 62% ethanol, and 35% n-betoxy ethanol solution, cooled to <-35°C with liquid nitrogen, or a solution of 5% perchloric acid, and 95% acetic acid glacial used at room temperature. To remove copper that redeposited on the discs during the electropolishing process, the discs were ion milled in a Gatan Dual Ion Mill (Model 600) at room temperature using two guns at a current of 0.5 to 2.0

milliamperes for ten minutes at an angle of 15 degrees. To characterize the microstructure and determine the bainite lath width, the samples were examined in a JEOL Model JEM 100 CX transmission electron microscope operated at 120 kV.

IV. RESULTS AND DISCUSSION

A. MECHANICAL BEHAVIOR

The David Taylor Research Center provided the author with data concerning the 0.2 percent yield strength, ultimate tensile strength, percent reduction in area, percent elongation, and Charpy V-notch impact energy of each specimen. These are shown in Table IV and Figure 10. Percent reduction in area and percent elongation are the two parameters used to analyze the ductility of each sample.

TABLE IV. HSLA-100, HSLA-100 WITH INCREASED COPPER, AND ULCB, AS-QUENCHED (WATER), STRENGTH AND DUCTILITY DATA.

	.2% YS (MPa)	Ult Tens Str (MPa)	% Elong (%)	% Red in Area (%)
HSLA-100	738	991.25	23.42	68.22
HSLA-100 w/incr copper	920.5	1117.0	16.5	65.0
ULCB	841.2	972.2	16.8	71.0

1. Strength and Ductility

When compared against the two other steels, HSLA-100 has less strength, but more ductility; an expected relationship. HSLA-100 with increased copper, which meets the design YS goal of 896 MPa, obtains a much

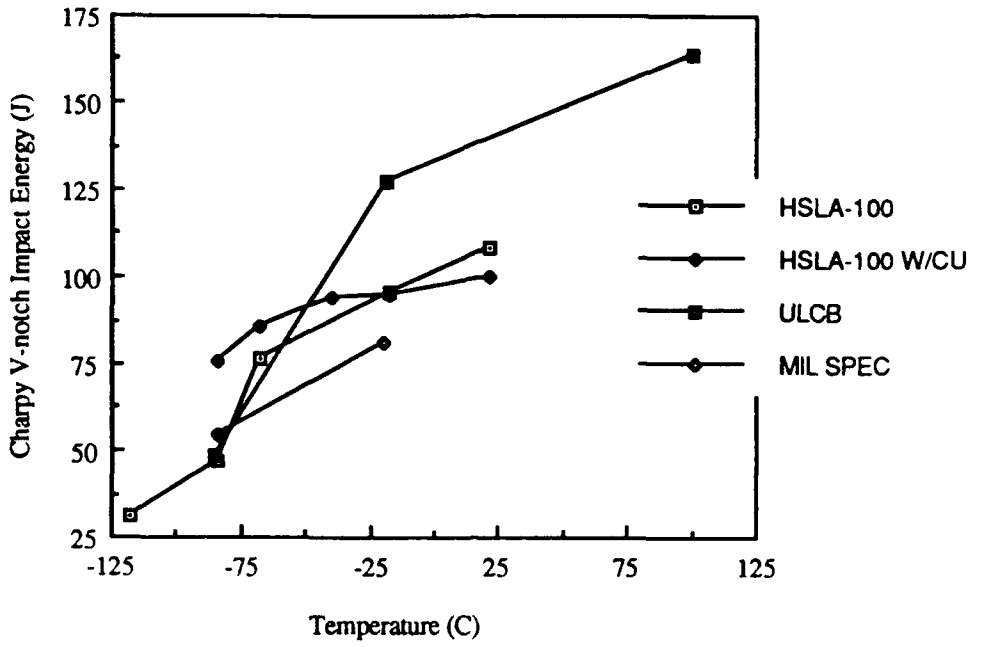

Figure 10. HSLA-100, HSLA-100 with Increased Copper, and ULCB, as-quenched (Water), Charpy Impact Behavior as a Function of Temperature.

higher level of strength with a corresponding large decrease in percent elongation and small decrease in percent reduction of area. The ULCB steel, which was also designed to reach the 896 MPa level but failed to meet it, has a strength slightly below that of the increased copper sample. However, the ULCB's percent reduction in area is the greatest for all three samples, while the percent reduction in area falls to its expected value between that of the HSLA-100 and increased copper samples. Accordingly, the ULCB is considered to be in a relatively more ductile condition than the other two.

2. Upper-Shelf Impact Energy and DBTT

The HSLA-100 specimen's upper-shelf energy is higher than that of the increased copper, but much less than the ULCB upper shelf energy. The HSLA-100 DBTT follows the same pattern; greater than the increased copper specimen, but less than the ULCB's upper-shelf energy. The wide disparity between DBTT for each steel causes a disparity in impact energy levels at the -19°C and -84°C military specification low temperature toughness design points. However, each of the as-quenched steels meets the required Charpy Impact energy levels (the ULCB is slightly lower than the military specification at -84.4°C, but is within 10% of the required value).

The ULCB specimen shows an upper shelf energy well above the other two samples. Since its strength is known to lie between that of the other two specimens, this seems to support the supposition that the ULCB steel is more ductile than its value of percent elongation indicates.

B. INCLUSION STUDY

In order to determine the composition, morphology, and distribution of non-metallic inclusions in the HSLA with increased copper and ULCB steels, polished, un-etched specimens were examined on both the optical and scanning electron microscopes. In order to provide a statistical analysis, 300 fields were examined from the HSLA-100 sample and 150 from the ULCB sample; all 450 fields at a magnification of 1000X. An EDX spectra was collected from each

observed inclusion to determine its composition, and photographs were taken at various magnification using both the optical microscope and SEM.

1. HSLA-100 With Increased Copper Steel

A total of 26 inclusions were observed with a mean diameter of 7.23 microns, median diameter of 6.0 microns, and a standard deviation of 6.55 microns (see Figure 11). The large standard deviation results from the fact that of the 26 total inclusions, six are above 10 microns in diameter and eight are below 3 microns. There was only one inclusion in the 7-8 micron range, where the "average" value was supposed to be located. The median diameter is therefore a better indication of "typical" inclusion size. The surface fraction, using this median diameter, was calculated to be .0331%.

There were 10 sulfide inclusions found with a 5.74 micron mean diameter, 2.0 micron median, and 8.43 micron standard deviation. Once again, the mean diameter is misleading because it is artificially increased by a single large inclusion. All but two of the inclusions are less than 4 microns (see Figure 12). Therefore, the median diameter of 2.0 microns is more indicative of the typical sulfide inclusion diameter. Only three of the sulfide inclusions observed were of the deleterious MnS long stringer type (see Figure 13 and Figure 14). Instead, the majority were characteristic of the small, hard, and spherical (Ca, Mn)S type. This type of inclusion is shown in Figure 15 with the accompanying EDX spectra provided in Figure 16.

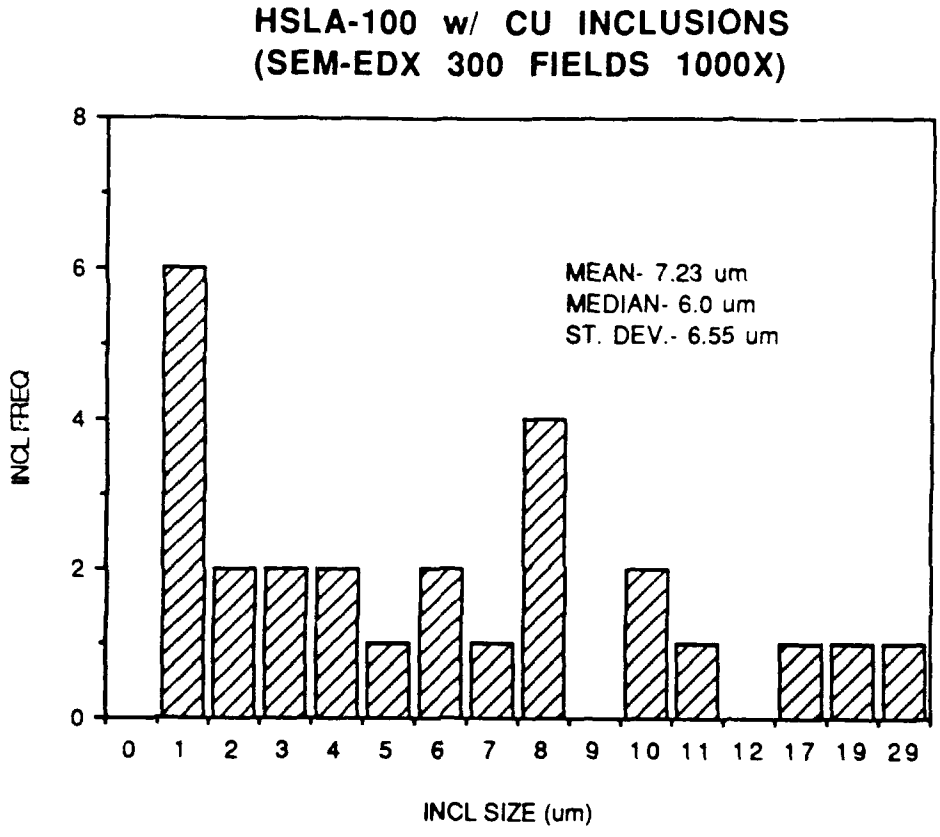

Figure 11. HSLA-100 With Increased Copper Inclusion Distribution From SEM-EDX Study.

There were only three pure oxide inclusions present within the 300 fields observed, and two of these were greater than 12 microns in diameter. Large oxide inclusions normally originate from exogenous sources (such as refractory material) can serve as crack initiation sites, and consequently, are considered harmful in most cases.

A second difficulty with oxide inclusions arises in both calcium treated and untreated steels in that pure alumina and high alumina calcium

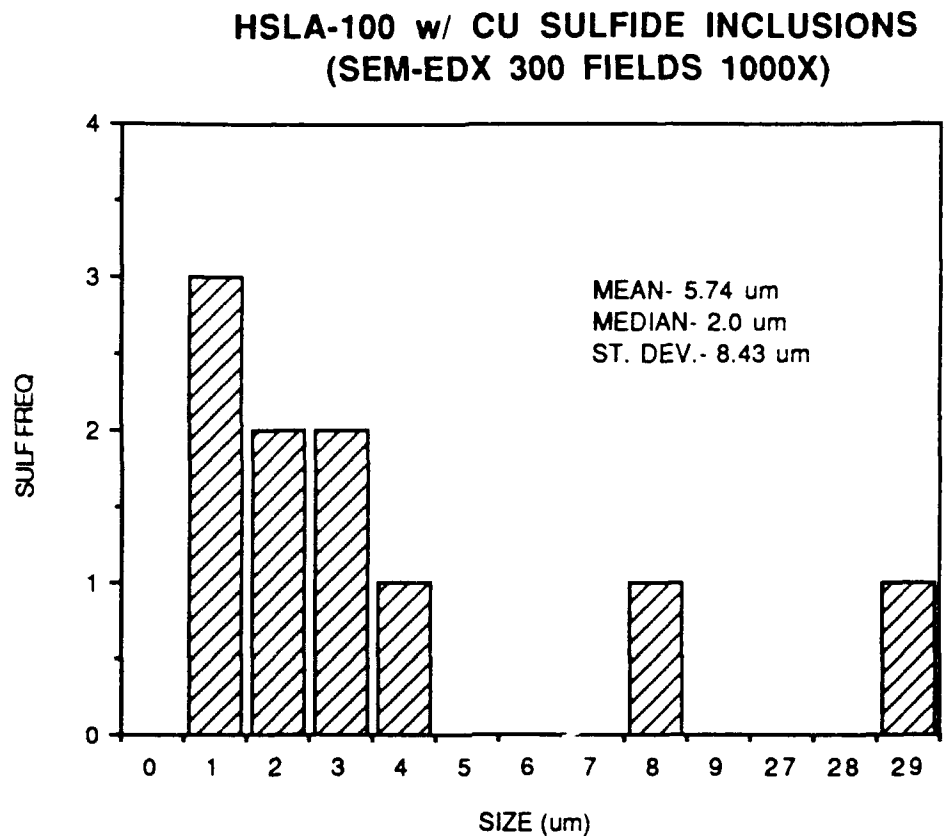

Figure 12. HSLA-100 With Increased Copper Sulfide Inclusion Distribution From SEM-EDX Study.

aluminates (e.g. $CaO\text{-}6Al_2O_3$) are relatively brittle and can break apart during rolling, creating detrimental anisotropic mechanical properties in the finished steel. If a great number of these broken calcium-aluminate clusters are present it may be indicative of an incomplete calcium treatment because there is not enough calcium present to result in the complete fluxing of the alumina galaxies [Ref. 31:p. 421]. Figure 17 is an example of one such inclusion. EDX

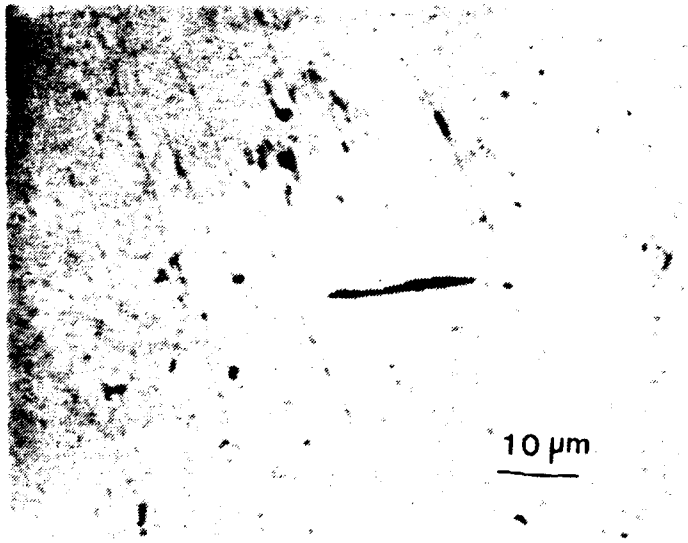

Figure 13. **Optical Micrograph of a MnS Stringer in HSLA-100 with Increased Copper Steel.**

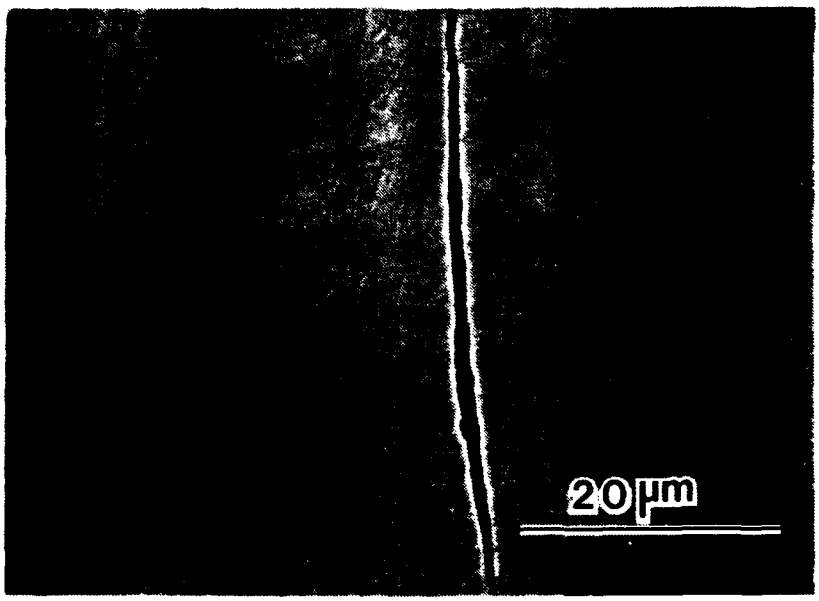

Figure 14. **SEM Micrograph of a MnS Stringer in HSLA-100 with Increased Copper Steel.**

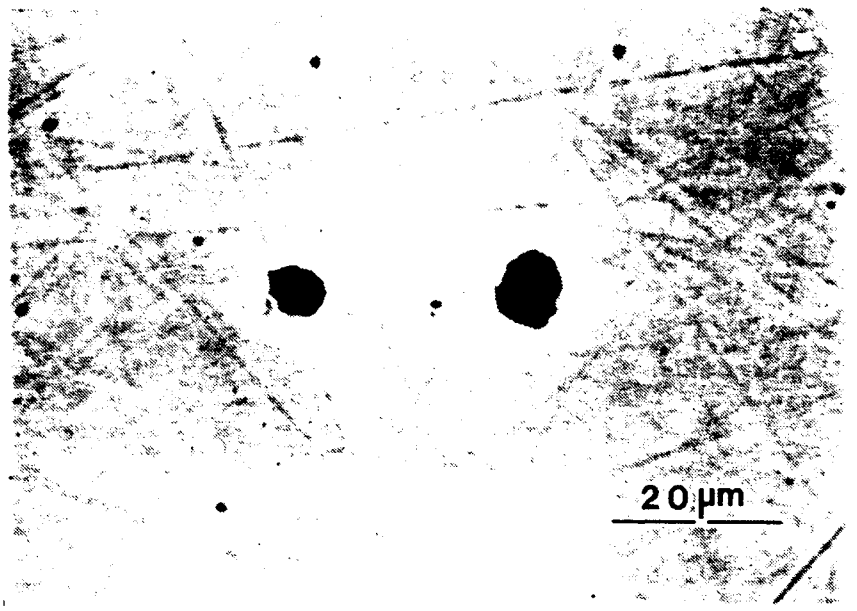

Figure 15. SEM Micrograph of a Ca(MnS) Inclusion in HSLA-100 with Increased Copper Steel.

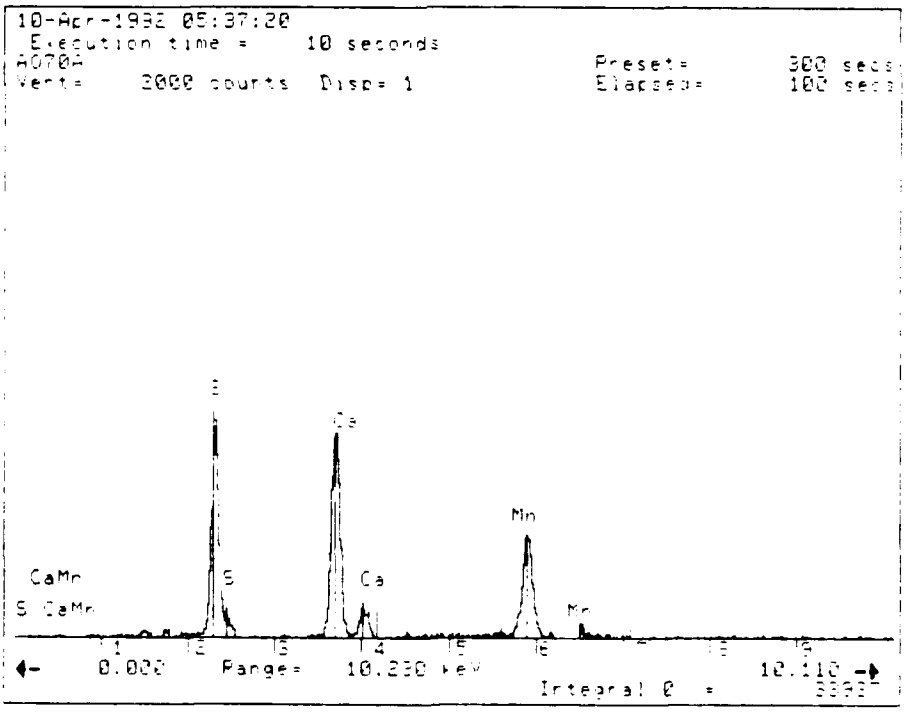

Figure 16. EDX Analysis of a Ca(MnS) Inclusion in HSLA-100 with Increased Copper Steel.

spectra showed the presence of both Ca and Al and analysis proved the material to be $CaO\text{-}2Al_2O_3$.

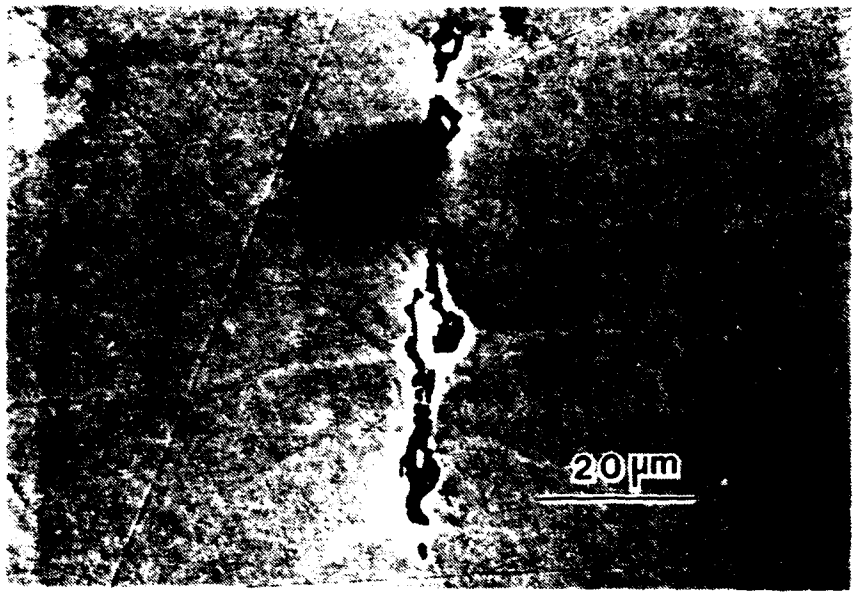

Figure 17. SEM Micrograph of a Calcium-Aluminate Inclusion in HSLA-100 with Increased Copper Steel.

Oxy-sulfide inclusions were the most frequently encountered inclusion type and had a mean diameter of 7.72 microns, median of 7.0 microns, and a relatively small standard deviation of 4.53 microns (see Figure 18). The majority of the oxy-sulfide inclusions were of the "bulls-eye" type prevalent in Ca-treated steels. The central, dark aluminate portion of the bulls-eye has solidified first and then the outer sulfide phase precipitated into it [Ref. 31:p. 421]. "Fishtailing" of these inclusions also often occurs, caused by rolling of the steel, with the tails pointing in the direction of rolling. Figure 19

a) and b) are examples of oxy-sulfide inclusions which display the characteristic "bulls-eye," and "fishtail." Analysis using data taken from the spectra shown in Figure 20 proved these inclusions to be $CaO\text{-}2Al_2O_3$ and corundum, and CaS as the surrounding second phase.

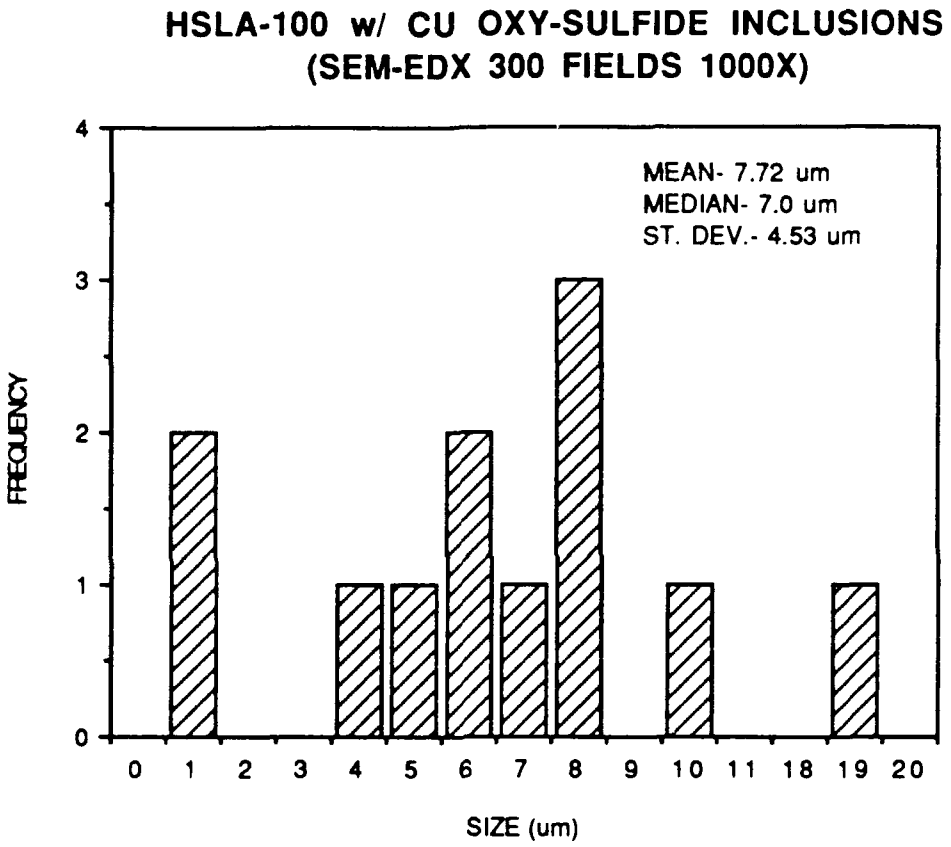

Figure 18. HSLA-100 With Increased Copper Oxy-Sulfide Inclusion Distribution from SEM-EDX Study.

Desulfurization and calcium treatment of steels complement one another in that if the sulfur content of the steel is kept to a minimum (0.006 wt% or below), there is little free sulfur to be trapped as CaS. However, other

a.

b.

Figure 19. **a) and b) SEM Micrographs of Oxy-Sulfide Inclusions Which Display the Two-Phase "Bulls-eye" Composition and "Fishtail Lipping" Caused by Rolling in HSLA-100 with Increased Copper Steel.**

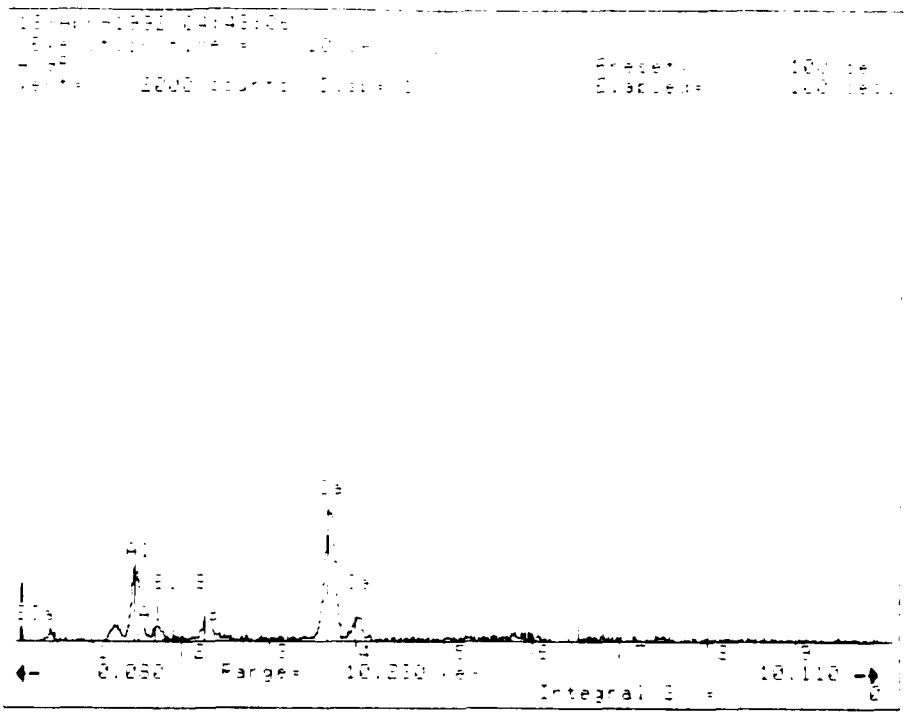

Figure 20. EDX Analysis of Oxy-Sulfide Inclusion in HSLA-100 with Increased Copper Steel.

researchers have shown that even the cleanest and most thoroughly calcium-treated steels will have a very small amount of MnS stringers. Accordingly, the sulfur treatment of this HSLA-100 with increased copper steel appears to have been effective; the sulfur content is 0.005 wt%, very few MnS stringers were found, and the upper shelf Charpy impact energy was relatively high.

The de-oxidation treatment by molten bath stirring, Al killing, and CaSi injections also appears to have been sufficient. Al-oxide arrays were not present, as evidenced by lack of large "clouds" and spectra containing mostly aluminum. A few broken calcium-aluminates were found, but most contained varying amounts of second phase CaS which makes the calcium-aluminates

more difficult to deform. Even though these two phase inclusions help in eliminating anisotropic mechanical properties, their size is frequently greater than 15 microns. Accordingly, these large inclusions could serve as crack initiation sites because of their slightly elongated shape, or tendency to separate from the parent matrix.

2. Ultra-Low Carbon Bainitic Steel

A total of 45 inclusions were found in the 150 SEM fields observed resulting in a mean inclusion diameter of 2.86 microns, median of 2.25 microns, and a standard deviation of 3.04 microns (see Figure 21). All except five of the inclusions are less than 4 microns in diameter; two are above 15 microns. The surface fraction. using the mean diameter, was calculated to be 0.026% of the area observed. The surface fraction of the ULCB steel sample is significantly less than the surface fraction of the HSLA-100 with increased copper specimen because even though the former's inclusion count was far greater than the HSLA-100's count, its average mean diameter was roughly a third that of the increased copper's inclusion mean diameter.

There were very few sulfides present and all were small and spherical in shape (< 3 microns) with a mean diameter of 1.86 microns. All sulfides proved to be MnS in composition with no calcium present. Also, there were no deleterious MnS stringers found. Figure 22 shows a micrograph of one of the sulfide inclusions with the accompanying EDX spectra (Figure 23).

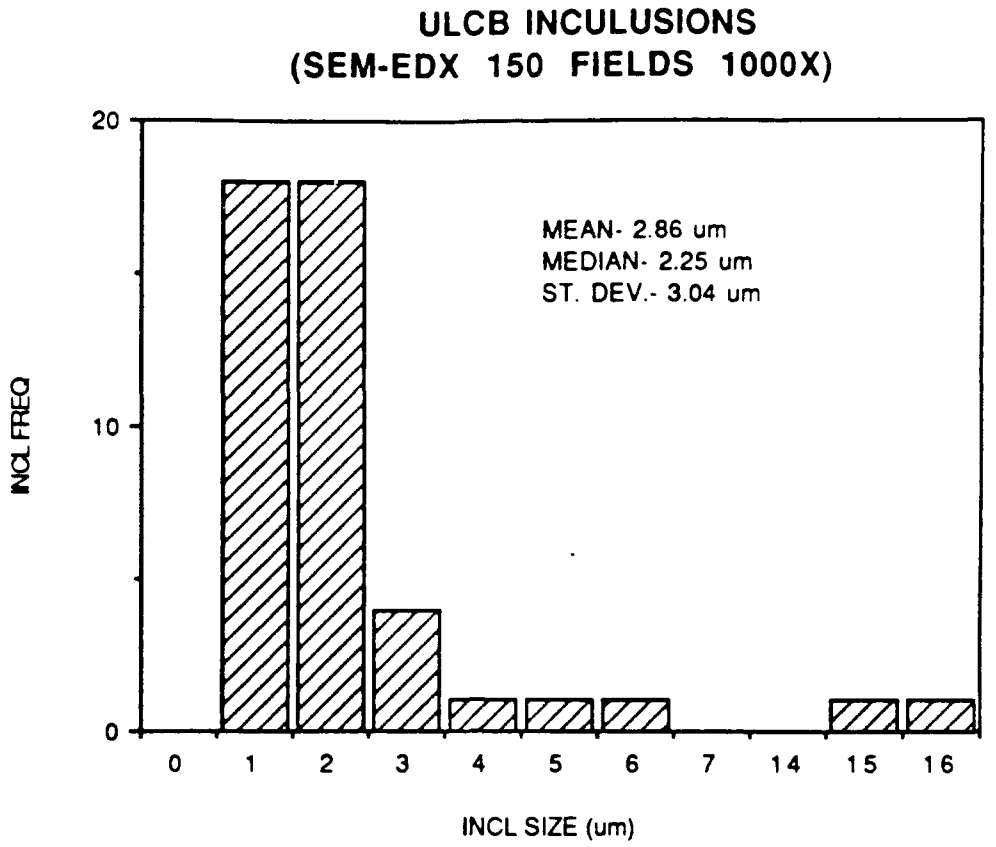

Figure 21. ULCB Inclusion Distribution From SEM-EDX Study.

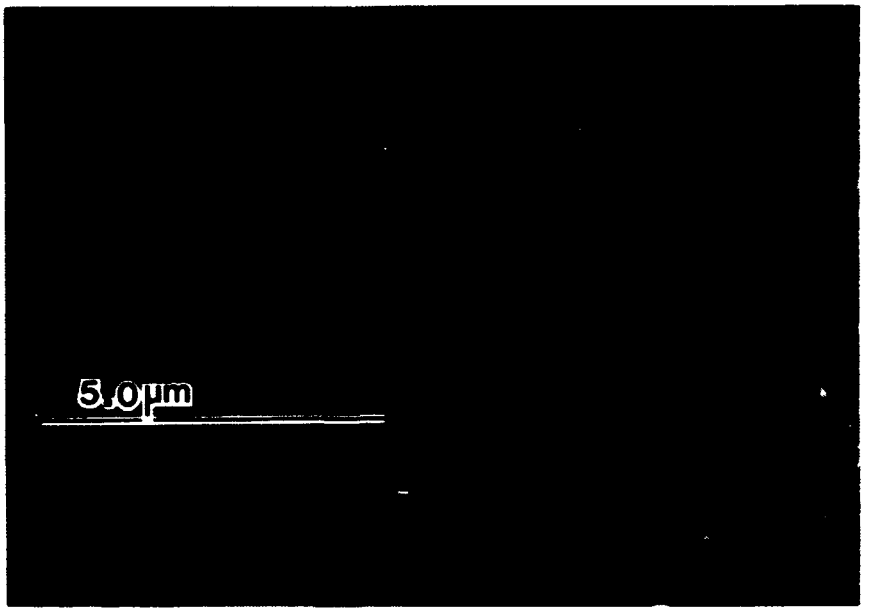

Figure 22. SEM Micrograph of a Sulfide Inclusion in a ULCB Steel.

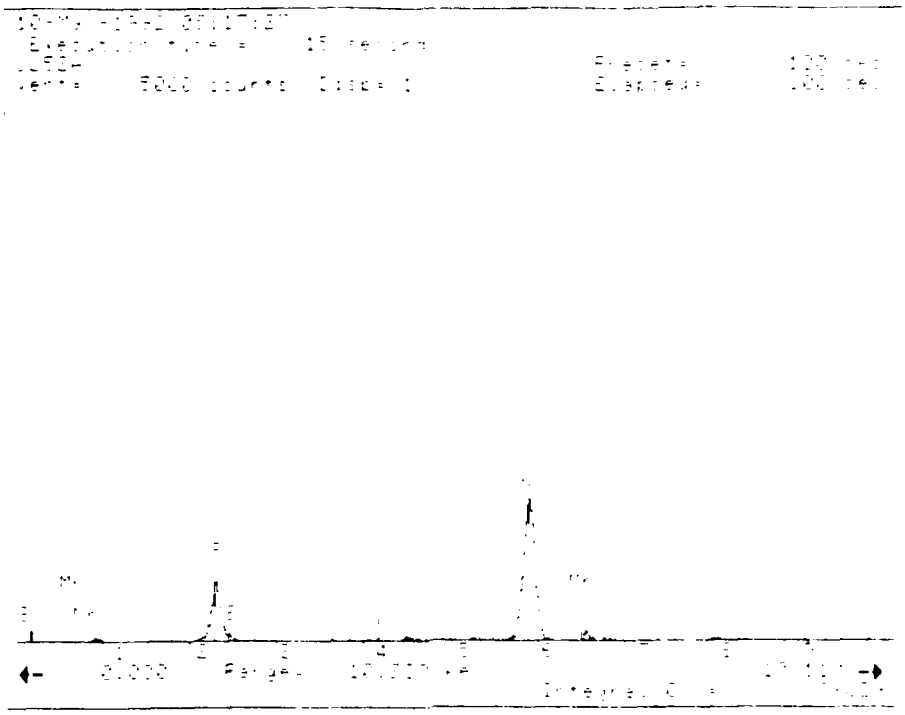

Figure 23. EDX Analysis of a Sulfide Inclusion in a ULCB Steel.

A little more than a third of the inclusions present were oxides. Even though most were small (12 between 1 and 2 microns in diameter), one large (> 16 microns) oxide array was present. A histogram showing oxide frequency vs. size is shown in Figure 24. EDX spectra showed the presence of Mn and Ti, but very little Al, and no Ca. There were no broken oxide stringers found. Analysis proved the oxide cloud to be composed of TiO_2 and MnO.

Over half of the inclusions present were oxy-sulfides with a mean diameter of 2.88 microns, median diameter of 1.75 microns, and a standard deviation of 2.79 microns (see Figure 25). The ULCB oxy-sulfide inclusions were similar to those found in the HSLA-100 specimen in that they were composed of two phases; an oxide core with a sulfide phase surrounding it.

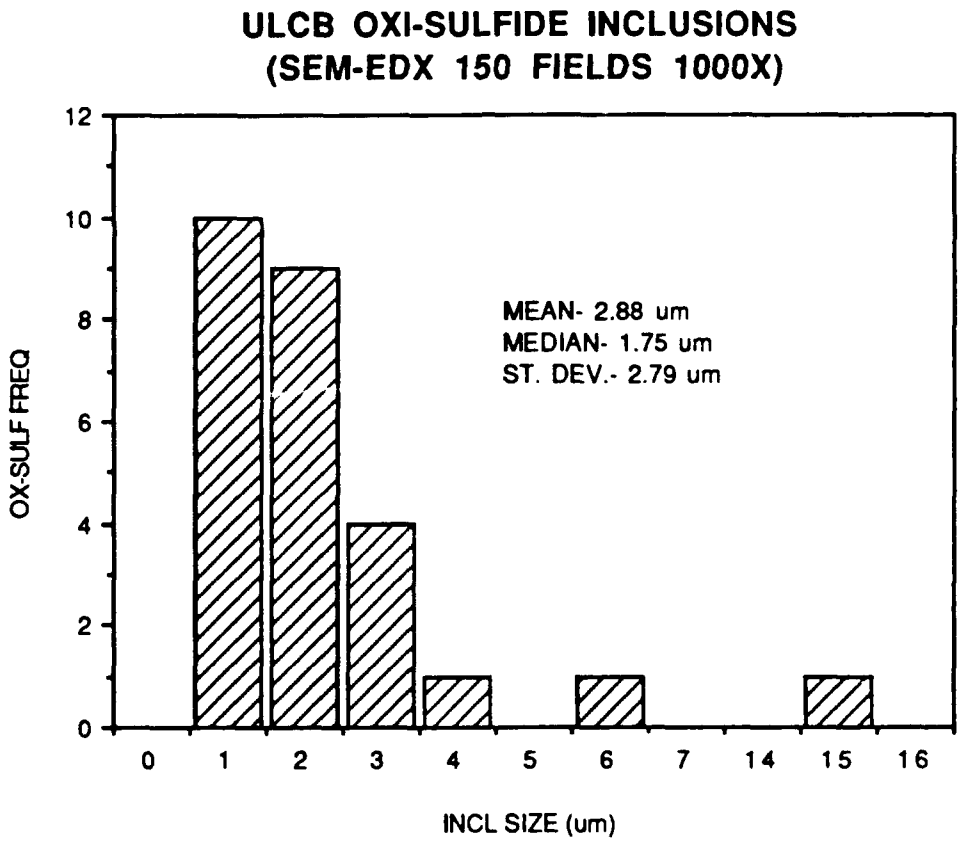

Figure 24. ULCB Oxy-Sulfide Inclusion Distribution From SEM-EDX Study.

However, they were much different in that the ULCB's oxide phase was composed of TiO_2, SiO_2 and MnO, and not Al_2O_3, and the sulfide phase was composed of MnS and not CaS. Figure 26 shows one of the two phase oxy-sulfide inclusions with the accompanying spectra (Figure 27). None of the ULCB inclusions show the "fishtail lipping," broken clouds, or elongation characteristic of inclusions after rolling.

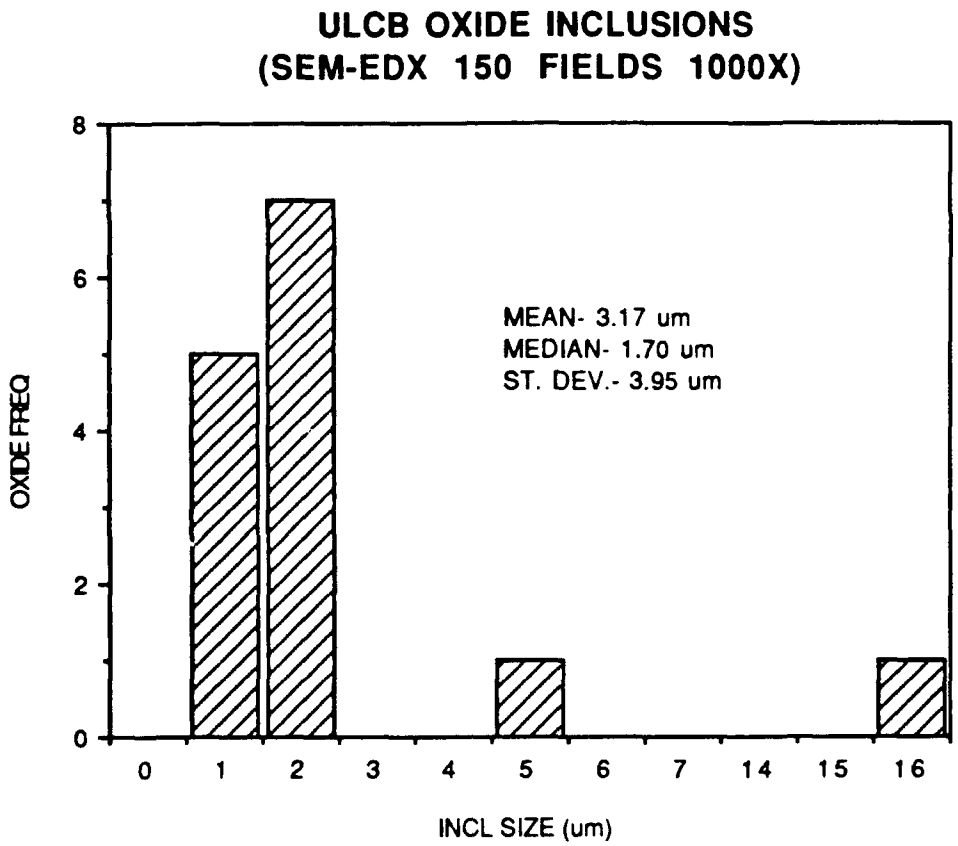

Figure 25. ULCB Oxide Inclusion Distribution From SEM-EDX Study.

The inclusion study shows that the ULCB steel was not aluminum killed, or calcium treated. This statement is supported by the absence of calcium, either in the form of CaS or CaO, and the minimal amount of aluminum present; the small amount which is present may be attributed to the original composition of the steel. The steel also was not thermo-mechanically processed. This is supported by the fact that even though there are MnS and oxide inclusions present, there were no deleterious MnS or oxide stringers

Figure 26. SEM Micrograph of an Oxy-Sulfide Inclusion in a ULCB Steel.

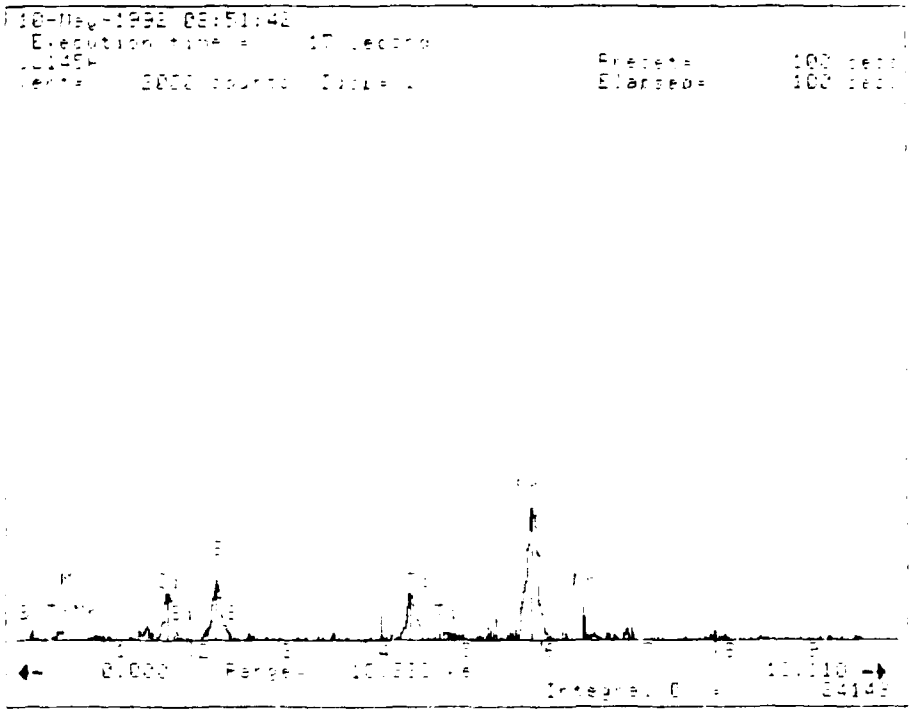

Figure 27. EDX Analysis of an Oxy-Sulfide Inclusion in a ULCB Steel.

found. Also, if the steel had been rolled, the oxy-sulfide inclusions would have been "lipped," broken, or elongated in the direction of rolling. Even though this steel has not been de-oxidized, or calcium treated, the inclusions are all small and relatively spherical, consequently, the mechanical properties should be isotropic. However, in its present condition, the steel plate could not be thermo-mechanically processed; a necessary step if it is to reach its design yield-strength goal of 896 MPa. Lastly, even though there were significant amounts of TiO_2, no titanium-nitrides (TiN) were found, which aid in making the transformation-product packet size small by pinning prior-austenite grain boundaries. A fine packet size is the key ingredient to attaining high levels of strength and toughness.

C. MICROSTRUCTURE

As-quenched and air cooled samples of HSLA-100, HSLA-100 with increased copper, and ULCB steels were examined using the optical microscope, SEM, and TEM in order to characterize their microstructures, and hence, examine the microstructural basis of their mechanical properties.

1. As-quenched HSLA-100 Steel

The light microscope and SEM investigation of the as-quenched HSLA-100 steel was made by Mattes and Comerford. They reported the transformation product to be lath martensite/retained austenite and acicular ferrite (bainite). The transformation product packet size was approximately 7

microns. Figure 28 and Figure 29 are optical and SEM micrographs showing the HSLA-100 as-quenched transformation product packets. [Ref. 12:p. 55] [Ref 9:p. 35].

The TEM showed a microstructure composed mostly of lath martensite and acicular ferrite with a small amount of retained austenite at lath boundaries. The retained austenite in these regions seems to have a carbon content of approximately 0.4 to 0.6 wt% as indicated by the frequent occurence of twin martensite. This high level of carbon occurs because as the acicular ferrite forms, it diffuses the carbon away from it thereby making the regions surrounding the acicular ferrite relatively rich in carbon. Also noted was a high dislocation density within each of the laths. The general microstructure is shown in Figure 30. Using this TEM image the average lath width was calculated to be 0.22 microns. Figure 31 is a TEM dark field image of retained austenite at lath martensite boundaries obtained by illuminating a spot in the selected area diffraction pattern (SADP); Figure 32 shows a TEM image of twin martensite.

Howell reported previously the presence of polygonal ferrite and copper precipitates in an oil-quenched HSLA-100 steel [Ref. 32:p. 902]. The water-quenched sample contained neither, nor did it contain coherent copper precipitates, as proven by the lack of streaking in the acicular ferrite/lath martensite SADP.

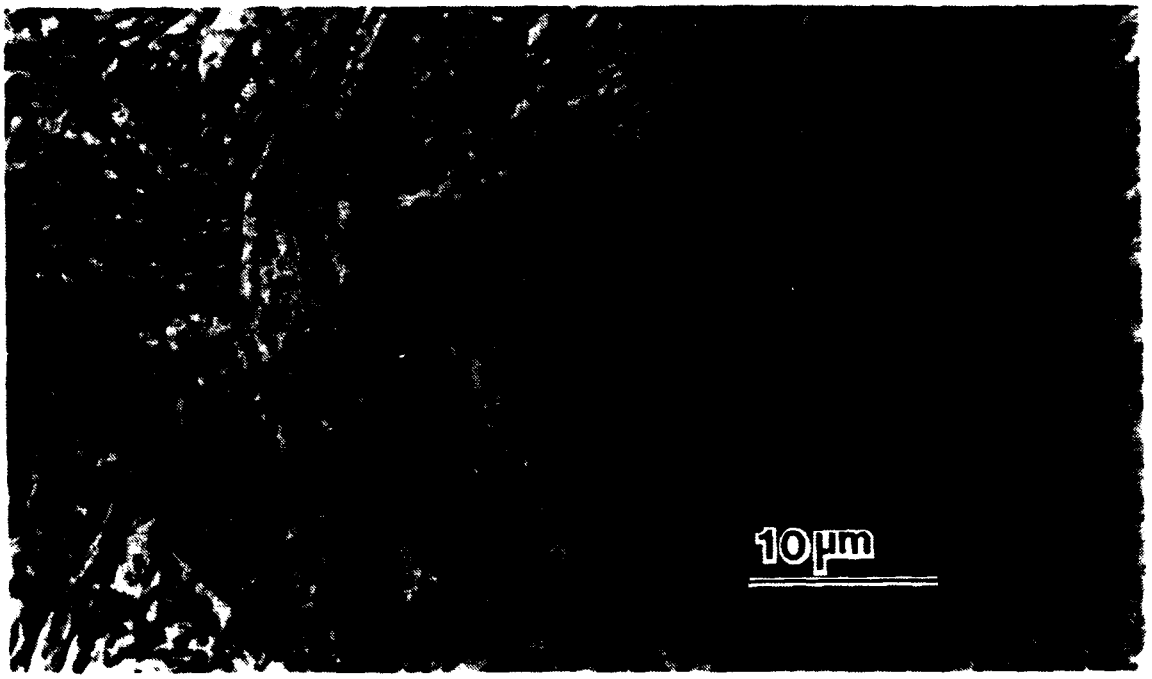

Figure 28. **Optical Micrograph of the As-quenched HSLA-100 Steel Transformation Product Packets.**

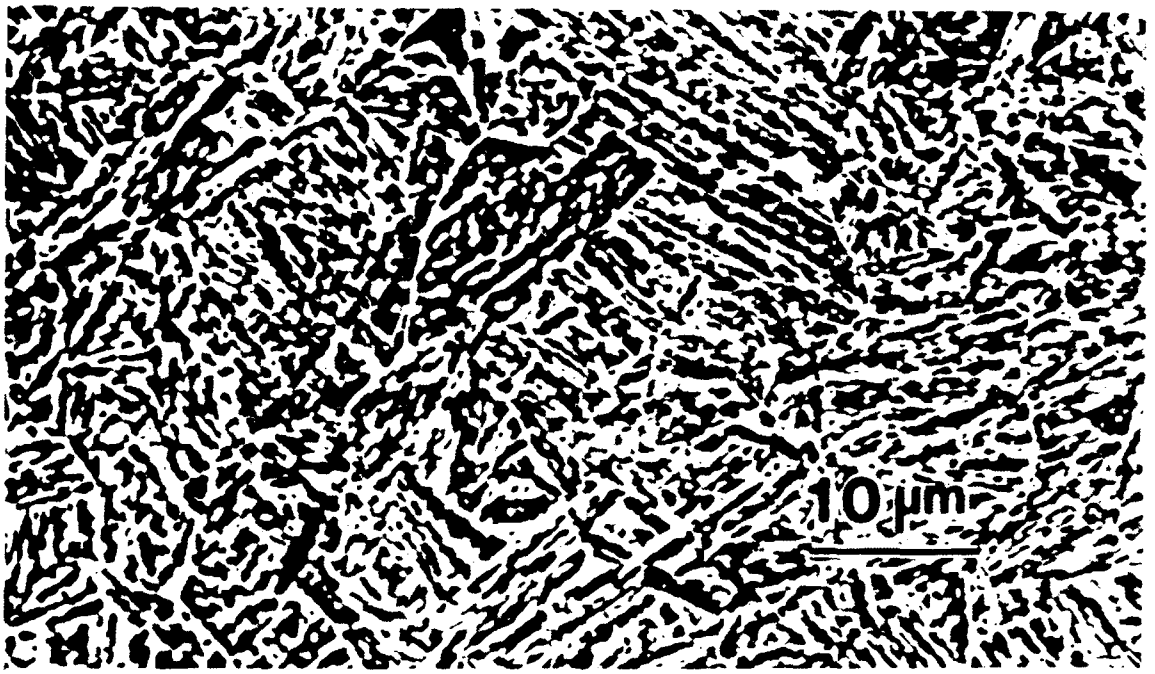

Figure 29. **SEM Micrograph of the As-quenched HSLA-100 Steel Transformation Product Packet.**

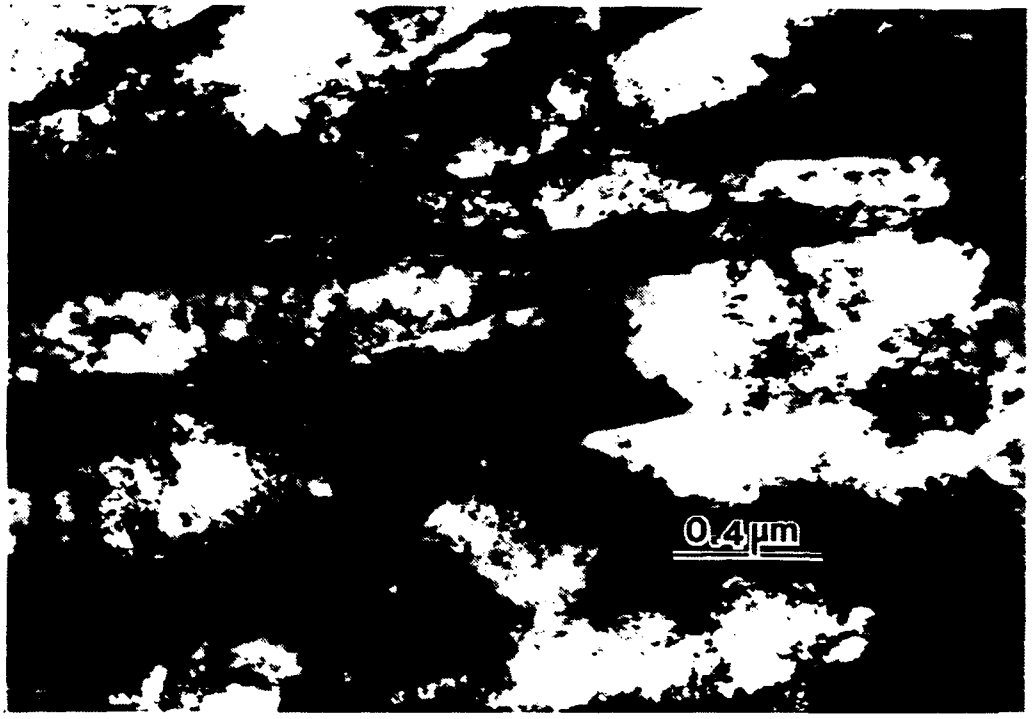

Figure 30. **TEM Micrographs of the General Microstructure of As-quenched HSLA-100 Steel Composed Lath Martensite, Acicular Ferrite, and Retained Austenite (Note the High Dislocation Density Within the Laths).**

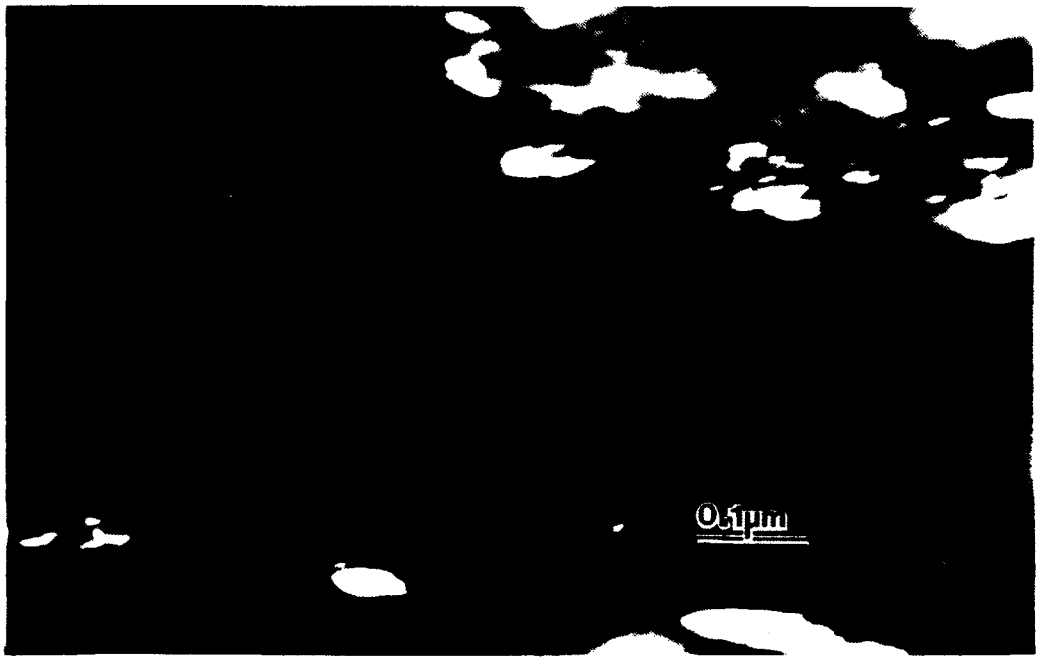

Figure 31. **TEM Image of Retained Austenite at Lath Martensite Boundaries in As-Quenched HSLA-100 Steel. Imaged Using g=220 of Austenite.**

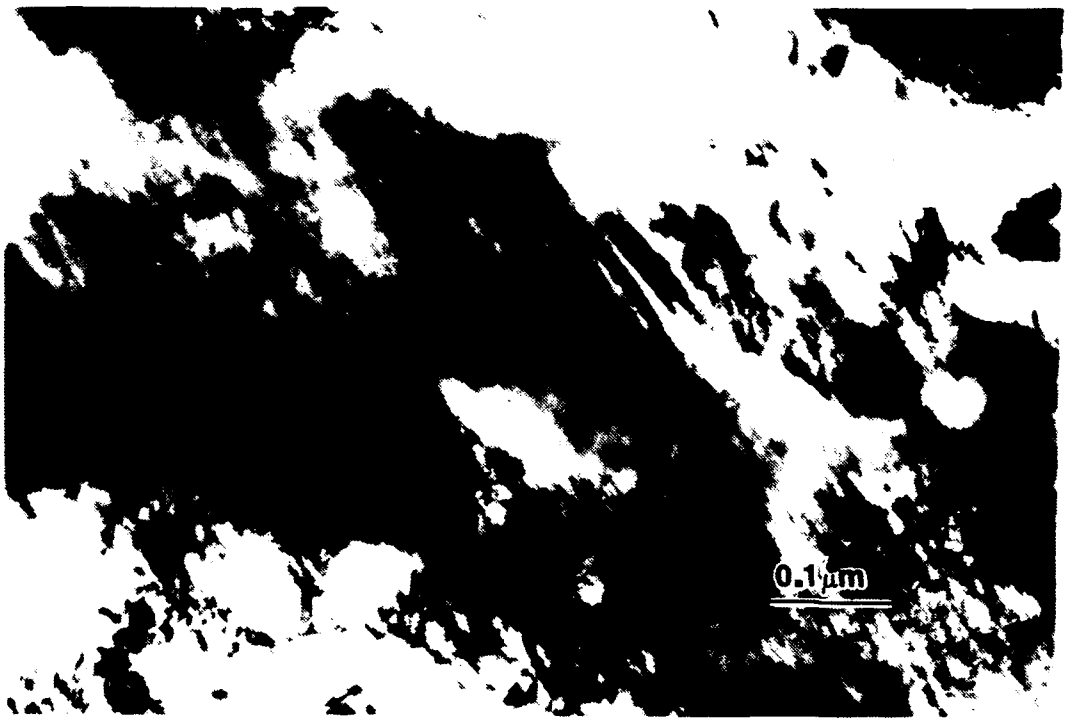

Figure 32. TEM Image of Twin Martensite in As-quenched HSLA-100 Steel.

The microstructural basis for the strength of the as-quenched HSLA-100 steel is the fine transformation product packet size, small lath width, and high dislocation density. The basis for its toughness is its fine transformation product packet size which is a result of the small "pancaked" prior austenite grains.

2. As-quenched HSLA-100 With Increased Copper Steel

The light microscope and SEM revealed an increased copper microstructure similar to that of the HSLA-100 sample. Transformation

product packets, similar in morphology to bainite packets in high-carbon steels, are shown in Figures 33 and 34. Using the SEM micrograph (at 1500X) the transformation product packet size was measured to be 7.01 microns. Also, "manganese banding" was viewed in the light microscope at a low magnification (Figure 35). Manganese banding is a macro-segregation of manganese, and is a result of the thermo-mechanical processing of the steel plate.

The TEM confirmed that the transformation product packets were composed of lath martensite and acicular ferrite with a small amount of retained austenite at lath boundaries (see Figures 36 and 37). The average lath width was calculated to be 0.227 microns. Martensite twinning was also frequently observed (Figures 38, 39 and 40).

Figure 33. Optical Micrograph of the As-quenched HSLA-100 Steel With Increased Copper Transformation Product Packets.

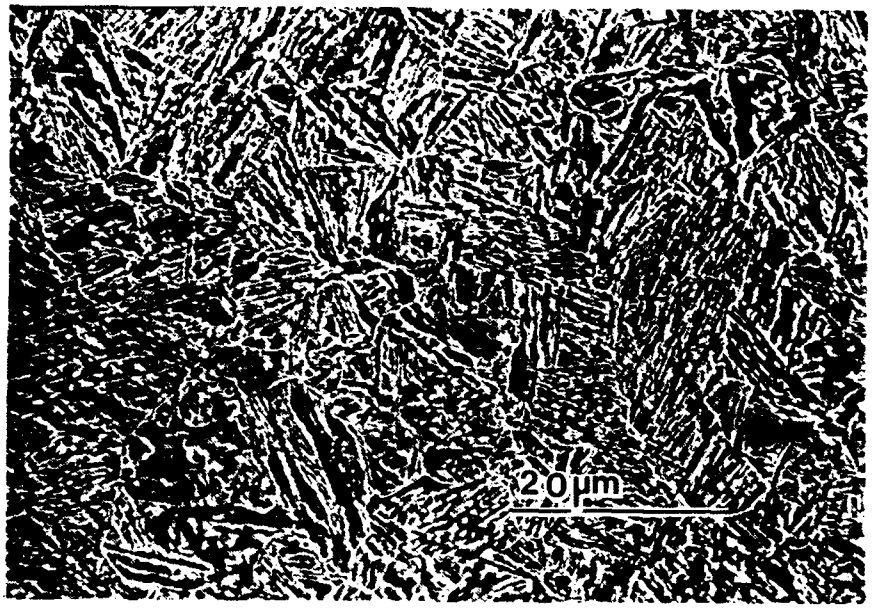

Figure 34. **SEM Micrograph of the As-quenched HSLA-100 Steel with Increased Copper Transformation Product Packets.**

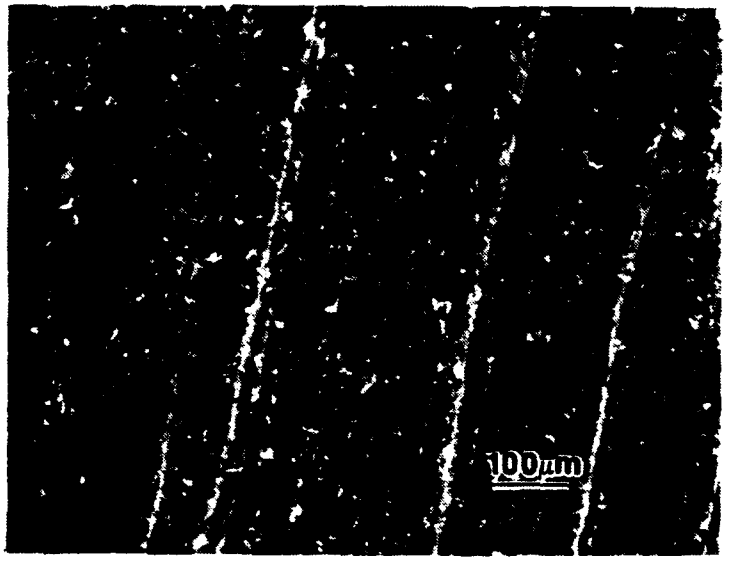

Figure 35. **Optical Micrograph of Manganese Banding in HSLA-100 Steel with Increased Copper Steel.**

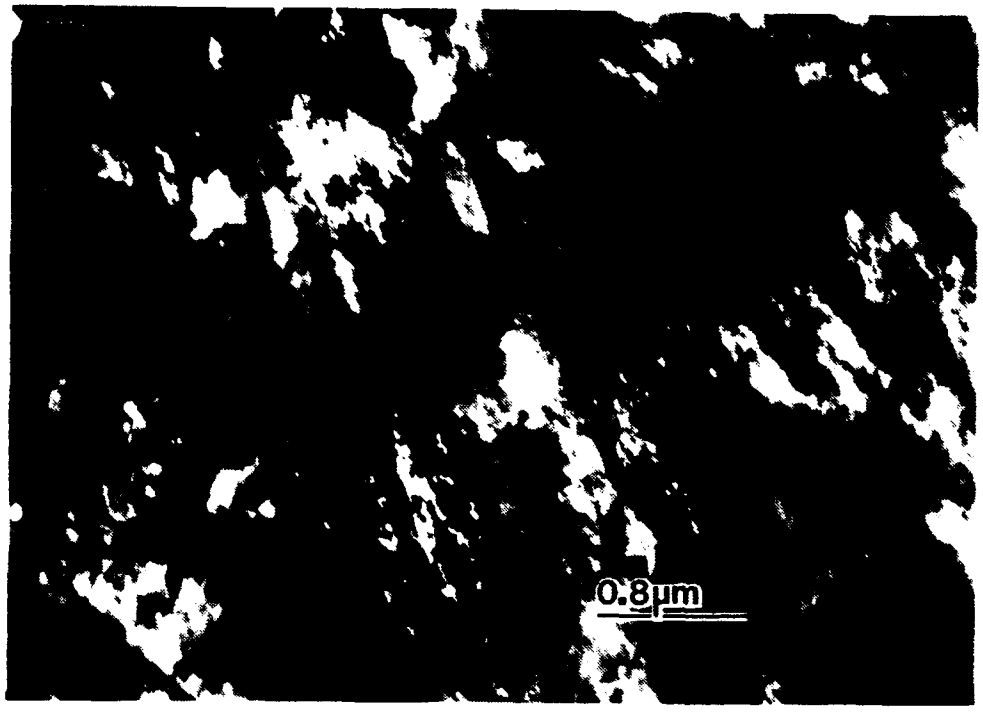

Figure 36. **TEM Micrograph of the General Microstructure of As-quenched HSLA-100 Steel With Increased Copper Steel Composed of Lath Martensite, Acicular Ferrite, and Retained Austenite.**

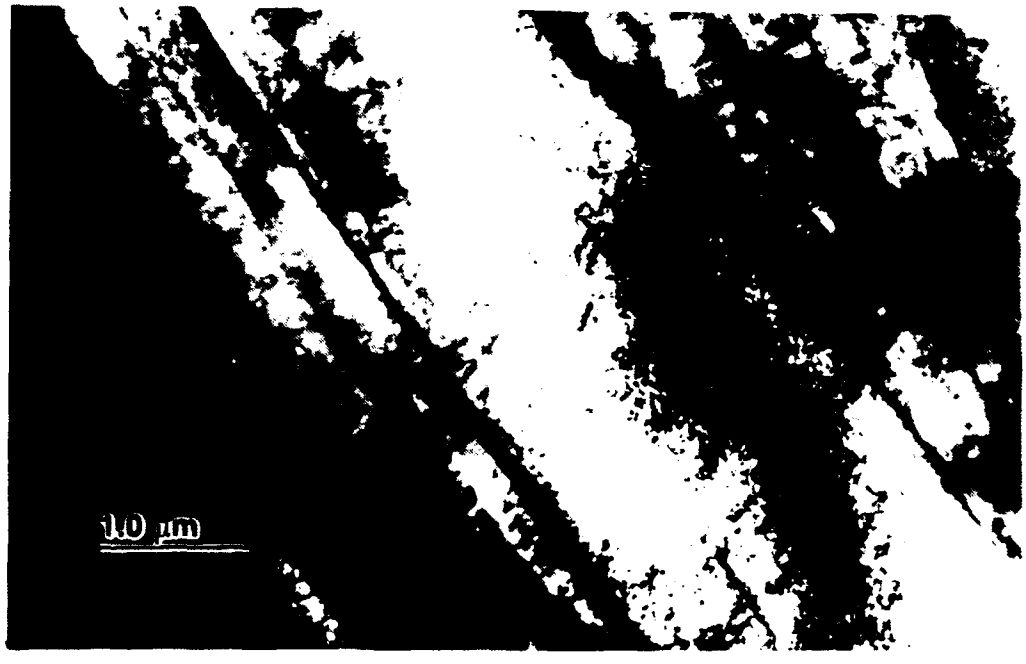

Figure 37. **TEM Image of Acicular Ferrite and Lath Martensite With Retained Austenite at Lath Boundaries in HSLA-100 With Increased Copper Steel.**

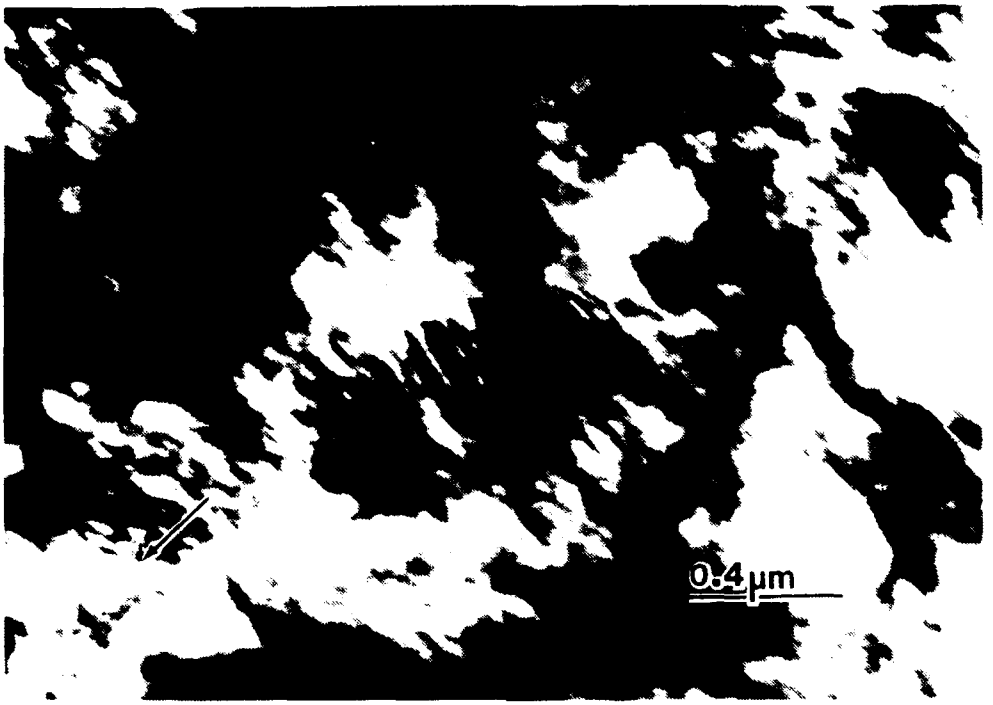

Figure 38. **TEM Image of Martensite Twinning in As-quenched HSLA-100 with Increased Copper Steel.**

Figure 39. **TEM Dark Field Image of Martensite Twinning in As-quenched HSLA-100 with Increased Copper Martensite Steel.**

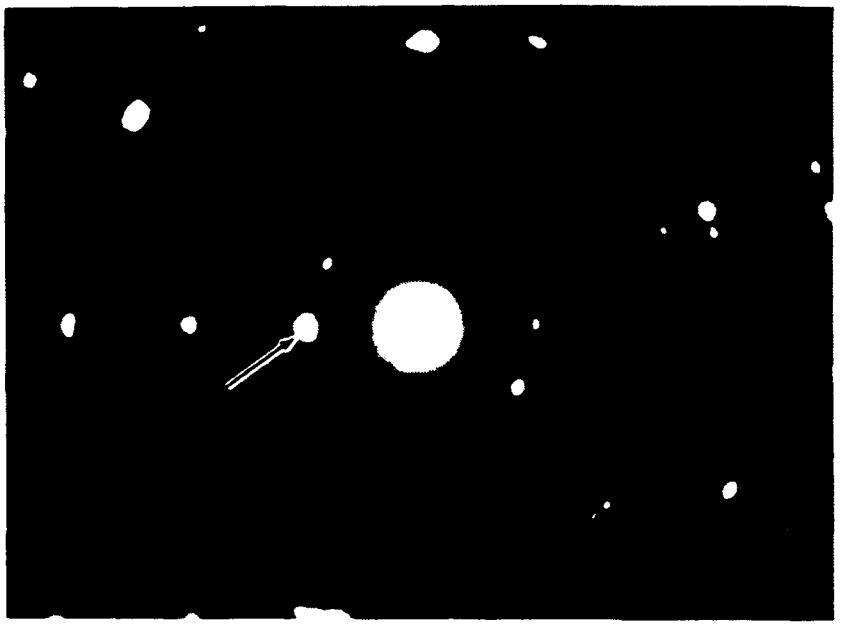

Figure 40. TEM Diffraction Pattern Characteristic of Twinning in HSLA-100 With Increased Copper Steel.

Surprisingly, ε-copper precipitates were found throughout the acicular ferrite and martensite laths; most frequently decorating dislocations. The precipitates congregated in large clouds, but within these large areas were homogeneously dispersed. This large dispersion of particles is contrary to findings by Howell, who reported ε-copper precipitates only at lath boundaries in oil-quenched HSLA-100 steel plate [Ref. 32:p. 902]. Figure 41 is a TEM image showing copper precipitates within an acicular ferrite lath decorating dislocations. Figure 42 shows the accompanying diffraction pattern which proved to be a b.c.c. [110] matrix orientation and a ε-copper [111] precipitate orientation pattern [Ref. 33:p. 809]. Figures 43 and 44 are bright and

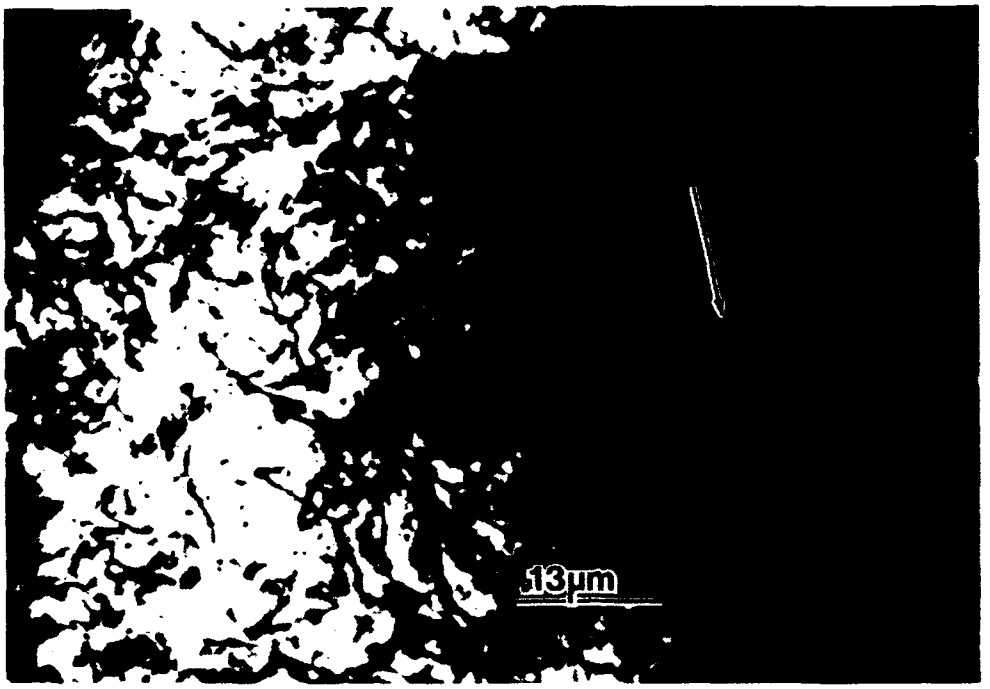

Figure 41. **TEM Image Showing Copper Precipitates Within an Acicular Ferrite Lath, Decorating Dislocations in an HSLA-100 With Increased Copper Steel.**

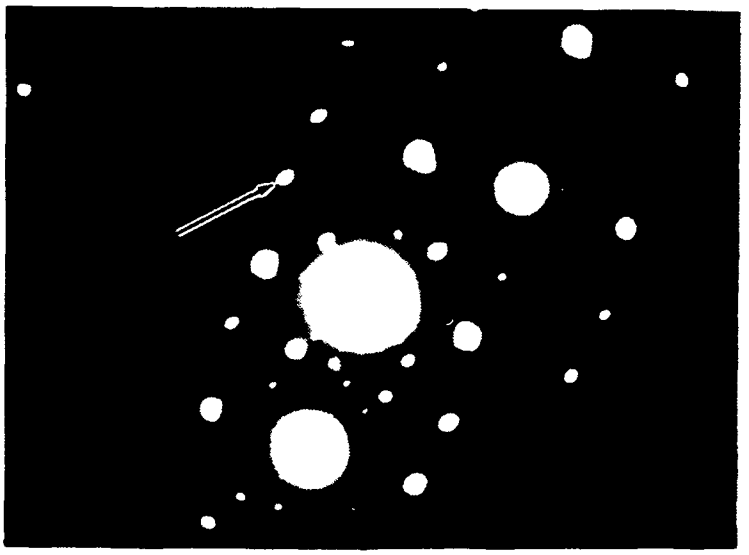

Figure 42. **Diffraction Pattern From an HSLA-100 With Increased Copper Steel of a [110] b.c.c. Zone Axis Close to a [111] f.c.c. ε-Cu Zone Axis. The Arrow Indicates a Cu[220] Spot.**

Figure 43. **Bright Field TEM Micrograph of Lath Martensite Containing ε-Copper Precipitates in HSLA-100 With Increased Copper Steel.**

Figure 44. **Dark Field TEM Micrograph of Lath Martensite Containing ε-Copper Precipitates in HSLA-100 With Increased Copper Steel.**

dark field TEM micrographs of lath martensite containing ε-copper precipitates. The maximum solubility of Cu in α-iron is 2.1 wt% at 850°C and the copper content of HSLA-100 with increased copper steel is only 2.0 wt%. It appears that the copper should not precipitate. However, because transformation from austenite to martensite/acicular ferrite occurs at a high degree of undercooling where the maximum solubility of copper is significantly lower, the copper can evidently precipitate out into the transformation products; resulting in the observed ε-copper precipitates. These small, ductile particles lead to increased levels of strength and toughness.

3. As-quenched ULCB Steel

The optical microscope and SEM showed a "bainite packet" morphology similar to both HSLA-100 and HSLA-100 with increased copper steels with the exception of size. The as-quenched ULCB transformation product packet diameter was calculated to be 12.4 microns, which is approximately twice the size of the HSLA-100 and HSLA-100 with increased copper steel's packets, and is only slightly smaller than the prior-austenite grain size. The larger packet size is a result of the material not being thermo-mechanically processed. If the prior-austenite grains had been "pancaked," (i.e. flattened) the number of nucleation sites would have been greatly increased with the resulting fine transformation product packet size caused by several packets sharing a single prior-austenite grain. Figures 45 and 46 are optical

and SEM micrographs of the as-quenched ULCB steel's transformation product packets.

The TEM showed the microstructure was composed mostly of lath martensite, some acicular ferrite, and a small amount of retained austenite (Figure 47). Also, a high dislocation density was noted in each of the laths, and the average lath width was found to be 0.201 microns. A small tin inclusion (composition determined by EDX analysis) was observed embedded in a martensite lath as shown by Figure 48; its origin is unknown.

The observed microstructure of lath martensite, acicular ferrite, and retained austenite is expected because of the amount of microalloying in the ULCB steel. However, the strength level does not meet 896 MPa design requirements because of the large transformation product packet size due to the material's lack of thermo-mechanical processing. The significantly higher toughness level attained is due to the reduced carbon content of the ULCB steel as compared to the HSLA-100 and HSLA-100 with increased copper steel. Lastly, the reduced lath width does not appear to have a significant impact on the strength level, particularly because the ULCB microstructure contains a high dislocation density, and dislocation motion will be impeded equally well by either a dislocation entanglement or a low angle lath boundary.

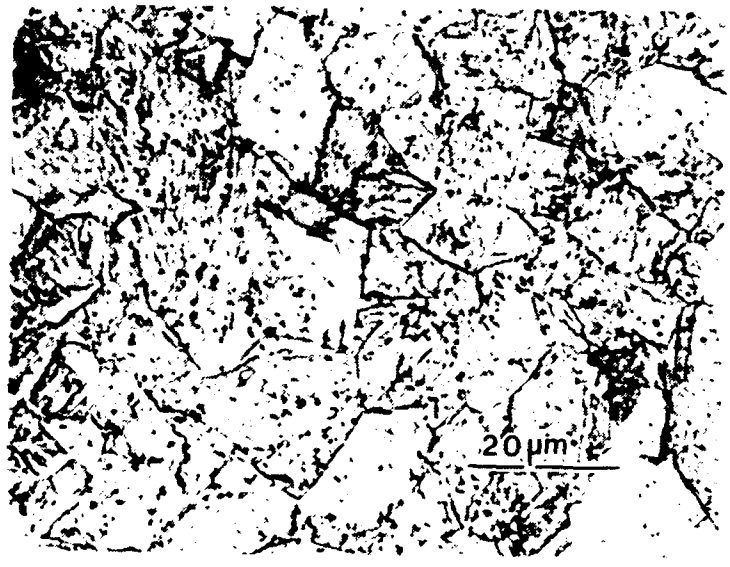

Figure 45. **Optical Micrograph of the As-quenched ULCB Steel Transformation Product Packets.**

Figure 46. **SEM Micrograph of the As-quenched ULCB Steel Transformation Product Packets.**

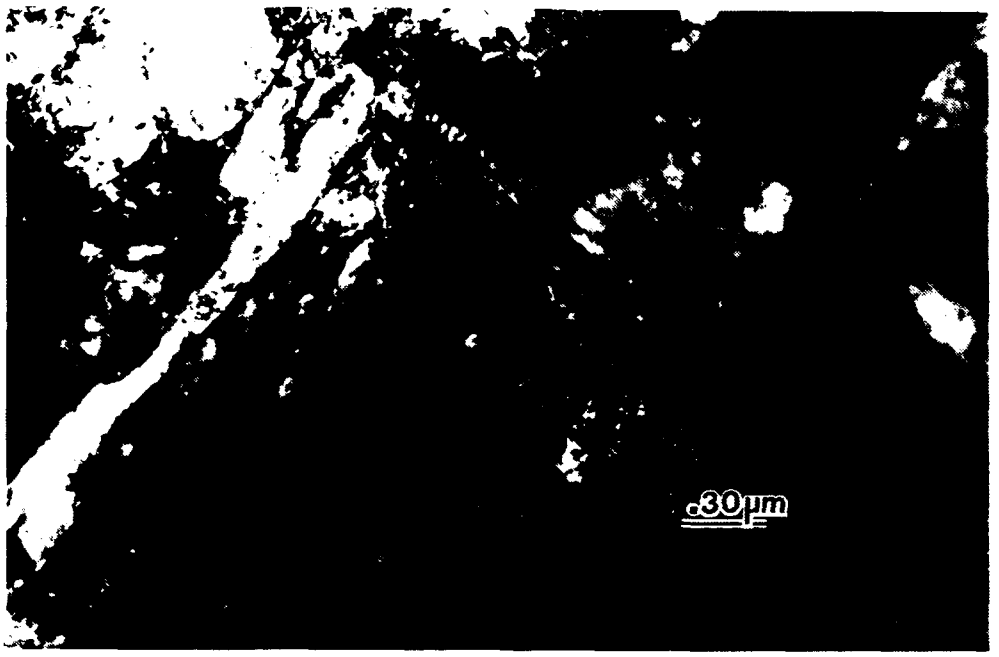

Figure 47. **TEM Micrograph Showing Lath Martensite, Acicular Ferrite, and Retained Austenite in an As-quenched ULCB Steel.**

Figure 48. **TEM Micrograph of a Tin Inclusion Embedded in Lath Martensite From an As-quenched ULCB Steel.**

4. Air-Cooled HSLA-100, HSLA-100 With Increased Copper, and ULCB Steels

The optical microscope, SEM, and TEM were used to investigate the microstructural impact of air-cooling on samples of HSLA-100, HSLA-100 with increased copper, and a ULCB steel. The optical microscope and the SEM showed that the ULCB air-cooled sample maintained its "packet" morphology similar to the morphology of the water-quenched sample (Figure 49). However, the transformation product packet size of the air-cooled sample was approximately half that of the water-quenched sample; 6.64 microns as compared to 12.40 microns, respectively. The HSLA-100 with increased copper steel showed less well-defined packets and fewer laths within the visible packet boundaries (Figure 50). Lastly, the HSLA-100 steel lost all packet definition and could be viewed as laths embedded in a dominant second phase (Figure 51).

The TEM confirmed that the ULCB transformation product packets were composed of lath martensite, acicular ferrite, a small amount of retained austenite, and a fine, homogeneously dispersed precipitate whose composition was not determined (Figures 52, 53, and 54). Polygonal ferrite was not present. This microstructure is consistent with the fact that the ULCB steel maintained its well defined packet morphology during air cooling.

The HSLA-100 with increased copper steel was composed of approximately equal amounts of acicular laths and pro-eutectoid ferrite, with

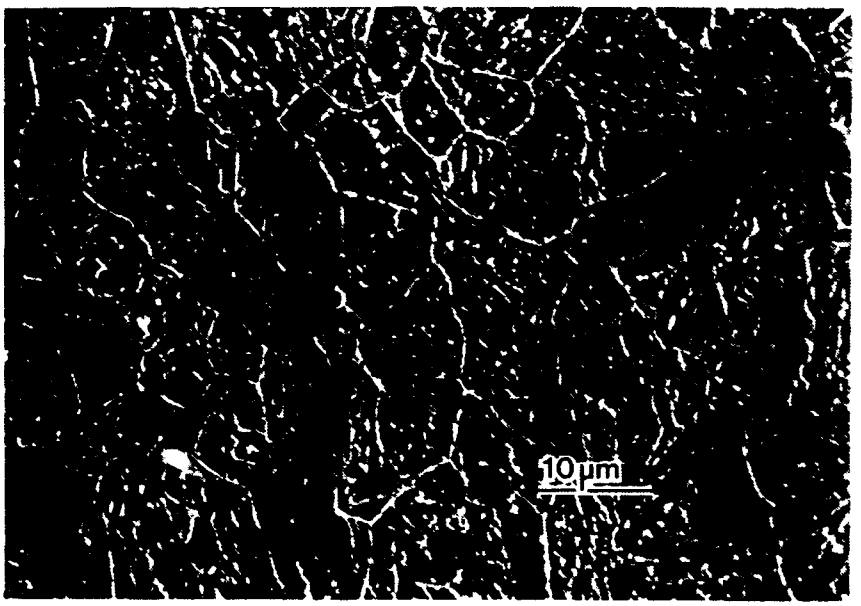

Figure 49. **SEM Micrograph of the Air-cooled ULCB Steel Transformation Product Packet.**

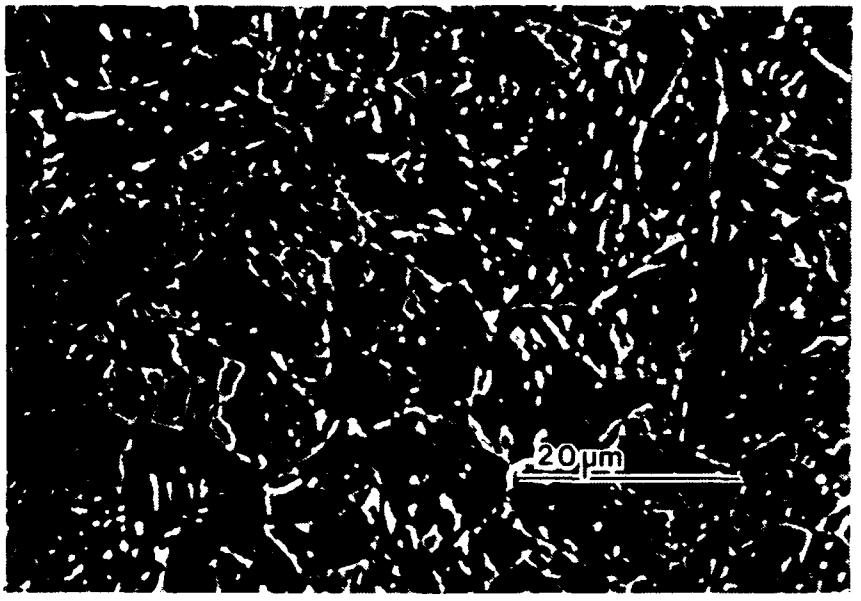

Figure 50. **SEM Micrographs of the Air-cooled HSLA-100 With Increased Copper Steel Transformation Product Packets.**

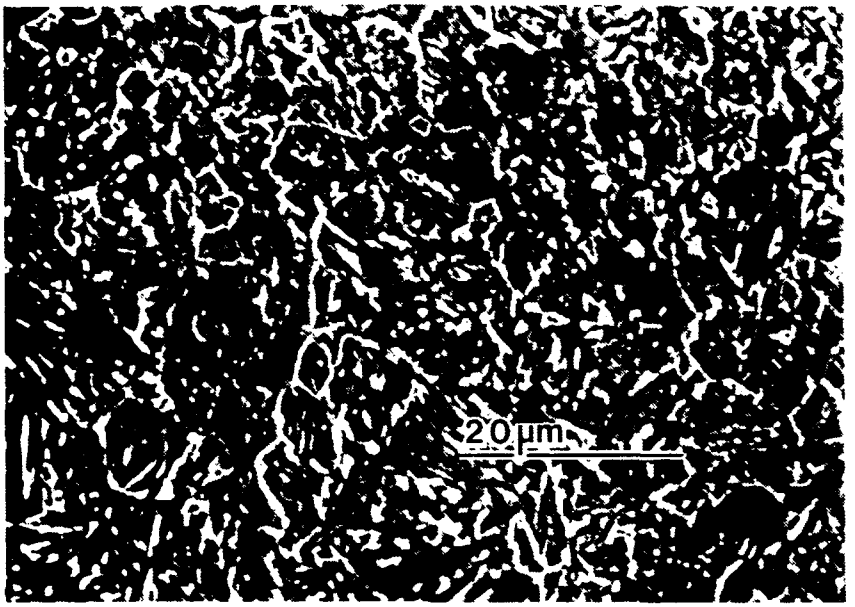

Figure 51. **SEM Micrograph of Laths Embedded in a Dominant Second Phase (Pro-eutectoid Ferrite) in an Air-cooled HSLA-100 Steel.**

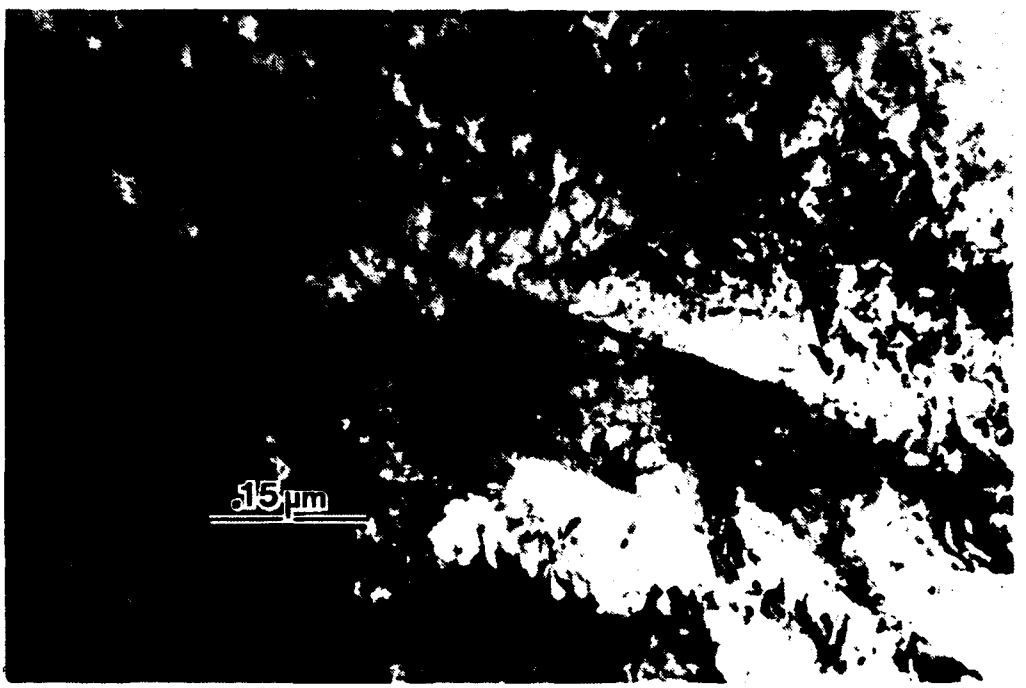

Figure 52. **TEM Micrograph of Lath Martensite, Acicular Ferrite, and Retained Austenite in an Air-cooled ULCB Steel.**

Figure 53. **Bright Field TEM Micrograph of Precipitates in an Air-cooled ULCB Steel.**

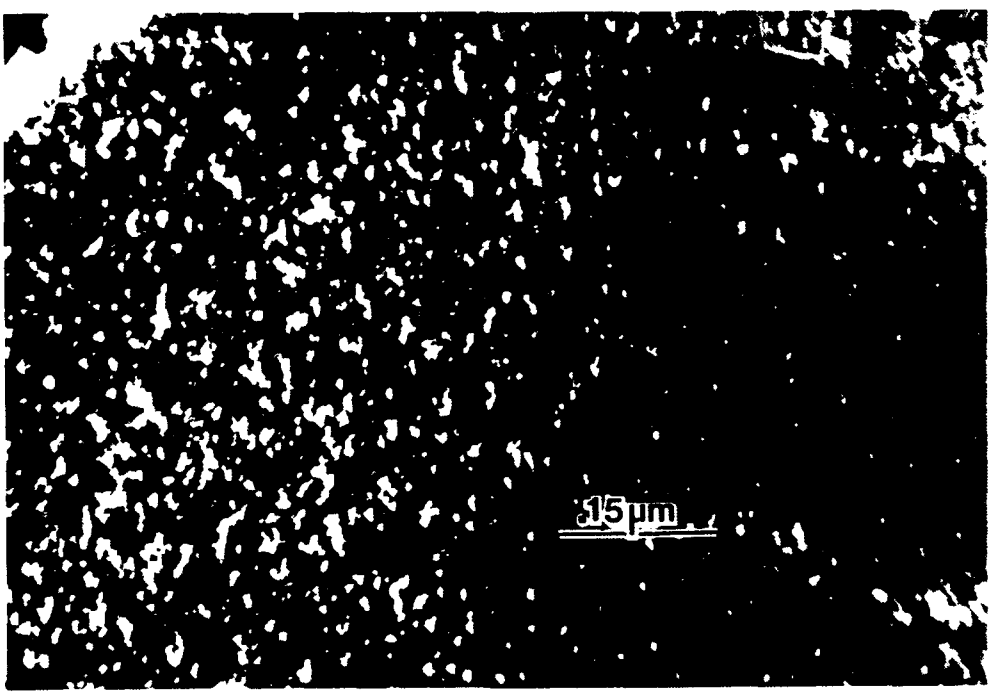

Figure 54. **Dark Field TEM Micrograph of Precipitates in an Air-cooled ULCB Steel.**

fine ε-copper precipitates dispersed throughout (Figures 55 and 56). The air-cooled HSLA-100 steel was composed of the same constituents as the air-cooled increased copper sample, with the exception that there were very few laths present embedded in a very dominant polygonal ferrite phase (Figure 57). All the polygonal ferrite observed was nearly free of dislocations. The appearance of the pro-eutectoid ferrite explains why the transformation product packets are less discernable in the HSLA-100 with increased copper, and are completely absent in the HSLA-100 sample.

The microstructural changes in HSLA-100, HSLA-100 with increased copper, and ULCB steels caused by air-cooling are expected because of the

Figure 55. TEM Micrograph of Lath Structures and Pro-eutectoid Ferrite in an HSLA-100 With Increased Copper Steel.

Figure 56. **TEM Micrograph of Lath Structures and Pro-eutectoid Ferrite With ε-Copper Precipitates in an HSLA-100 With Increased Copper Steel.**

Figure 57. **TEM Micrograph of a Lath-like Structure Embedded in Pro-eutectoid Ferrite in an HSLA-100 Steel.**

relative amount of microalloying done to each steel and the resulting location of the polygonal ferrite "C-curve" on the CCT diagram. The higher alloying of the ULCB steel has prevented the cooling rate from passing through the pro-eutectoid ferrite area while the least alloyed HSLA-100 steel has resulted in a microstructure consisting of nearly 100% polygonal ferrite. Pro-eutectoid ferrite will adversely affect a steel's strength because of its lower dislocation density when compared to that of lath martensite or acicular ferrite.

The smaller transformation product packet size in the ULCB steel is a result of the slower cooling rate providing for a better combination of nucleation and growth of the acicular ferrite/lath martensite packets, resulting in prior-austenite grains being shared by two to three transformation product packets. The smaller packet size as a result of air-cooling is an important observation because while still obtaining the desired finely divided microstructure, the large expense incurred by water-quenching steel plate immediately following t' ; final hot-rolling pass could be avoided.

V. SUMMARY

A. CONCLUSIONS

1. Mechanical Properties

The as-quenched HSLA-100, and HSLA-100 with increased copper meets the strength, ductility, and toughness (within 10%) requirements set forth by the HSLA-100 and HY-130 military specifications. The as-quenched ULCB steels meets the desired ductility, and toughness (within 10%) goals but fails to attain the required level of strength demanded by the HY-130 milspec.

2. Inclusion Study

The HSLA-100 with increased copper steel was adequately sulfur treated and deoxidized, as shown by the steel's low sulfur content, few MnS stringers, and lack of large oxide arrays. The ULCB steel was not calcium treated or aluminum killed; analysis failed to show either CaO or CaS in any of the inclusions and there was a minimum amount of aluminum present. The ULCB steel was also not thermo-mechanically processed. None of the inclusions found were either lipped or broken, and the MnS present was globular in shape. If the ULCB steel were to be hot-worked to raise its strength level, it would have to be de-oxidized and calcium treated to eliminate the MnS and pure oxide inclusions currently found in the steel.

3. Microstructure

The microstructural basis for the strength of the as-quenched HSLA-100, and HSLA-100 with increased copper steels is the fine transformation product packet size, small lath width, and high dislocation density. The increased copper steel contained fine, evenly dispersed ε-copper precipitates which adds to its high level of strength and toughness. The as-quenched ULCB steel did not reach the desired strength level because its transformation product packet size was too large; approximately the same size as the prior-austenite grains. Thermo-mechanical processing of the steel would result in a finer packet size by "pancaking" the prior-austenite grains.

Air-cooling of the ULCB steel caused very little apparent change in the make-up of the constituent microstructure, but reduced the transformation product packet size by half. Air-cooling of the HSLA-100 with increased copper steel introduced a significant amount of pro-eutectoid ferrite to the microstructure together with acicular ferrite. In the HSLA-100 steel, air-cooling caused polygonal ferrite to become the dominant phase. Polygonal ferrite will reduce the strength level of the steel because of its low dislocation density, and lack of a finely divided lath sub-structure.

B. RECOMMENDATIONS

1) Obtain continuous-cooling transformation (CCT) curves for the HSLA-100 with increased copper, and ULCB steels. Also, measure the cooling rates

of water-quenched, oil-quenched, and air-cooled samples and full steel plate to obtain the approximate positions on the CCT diagram. These two investigations will enable exact correlation between cooling rate and microstructure.

2) Study the effect that ε-copper precipitates present in the high copper HSLA-100 steel have upon further aging kinetics and mechanical properties. This would help determine the correct aging treatment for the best combination of strength and toughness obtainable from this steel.

3) Quantify the dislocation density present in various HSLA/ULCB steels, and relate the results to microstructure, cooling rate, and mechanical properties thereby enabling the best use of this very important strengthening mechanism.

LIST OF REFERENCES

1. Czyrca, Ernest J., *Development of Low-Carbon, Copper-Strengthened HSLA Steel Plate for Naval Ship Construction,* DTRL-SME-90/21, June 1990.

2. Gudas, John P., *Pre-certification Development Plan - HSLA-130 for Submarine Construction,* David Taylor Research Center, Metals and Welding Division, Annapolis, Maryland, March 1989.

3. Garcia, C.I., Lis, A.K., and Deardo, A.J., *The Physical Metallurgy of Ultra-Low Carbon Bainitic Plate Steels,* The Minerals, Metals, and Materials Society, pp. 451-467, 1990.

4. Porter, L.F., and Repas, P.E., "The Evolution of HSLA Steels," *Journal of Metals,* pp. 14-21, April 1982.

5. Blicharski, M.R., Garcia, C.I., Pytel, S., and Deardo, A.J., *Structure and Properties of ULCB Plate Steels for Heavy Section Applications, Processing, Microstructure and Properties of HSLA Steels,* A.J. Deardo, ed., The Minerals and Metals Society, pp. 317-331, 1978.

6. Araki, T., *Microstructural Strengthening Mechanisms in High Strength Low Alloy Steels,* Kobe Steel Ltd., Tokyo, Japan, pp. 259-271.

7. Czyrca, E.J., and Link, R.E., *Fracture Toughness of HSLA-100, HSLA-80, and ASTM A710 Steel Plate,* DTRC-SME-88164, January 1990.

8. Kirkwood, P.R., "A Viewpoint on the Weldability of Modern Structural Steels," *Proceedings of an International Symposium on Welding Metallurgy,* The Metallurgical Society, pp. 21-45, February 22-26 1987.

9. Mattes, V.R., "Microstructure and Mechanical Properties of HSLA-100 Steel," Master's Thesis, Naval Postgraduate School, Monterey, California, December 1990.

10. Bucher, J.H., Hamburg, E.G., and Wilson, A.D., *Symposium on Toughness Characterization and Specifications for HSLA and Structural Steels*, The Metallurgical Society of AIME, March 1977.

11. Coldren, A.P., and Cox, T.B., *Development of 100 ksi Yield Strength HSLA Steel,* DTNSRDC/SME-CR-07-86, July 1986.

12. Comerford, L.W., "A Study of the Microstructural Basis for the Strength and Toughness Properties of the Overaged HSLA-100 Steel," Master's Thesis, Naval Postgraduate School, Monterey, California, June 1991.

13. Irving, R.R., "Microalloying: The Route to Stronger, Tougher Steels," *Iron Age,* Vol. 226, no. 5, pp. 41-45, February 1983.

14. Pickering, F.B., *Physical Metallurgy of the Design of Steels,* Applied Science Publishers, Ltd., London 1978.

15. Wilson, A.D., Hamburg, E.G., Calvin, D.J., Thompson, S.W., and Krauss, G., "Properties and Microstructures of Copper Precipitation Aged Plate Steels, Microalloyed HSLA Steels," *Proceedings of Microalloying '88,* ASM International, pp. 259-274.

16. Czyrca, E.J., Link. R.E., Wong, R.J., Aylar, D.A., Montemaro, T.W., and Gudas, J.P., "Development and Certification of HSLA-100 Steel for Naval Ship Construction," *Naval Engineers Journal,* pp. 63-104, May 1990.

17. Hertzberg, R.W., *Deformation and Fracture Mechanics of Engineering Materials,* 3rd ed., John Wiley and Sons, Inc., 1989.

18. LeMay, I., and Schetky, L.M., *Copper in Iron and Steel,* John Wiley and Sons, Inc., New York.

19. Edmons, D.V., and Cochrane, R.C., "Structure Property Relationships in Bainitic Steels," *Metallurgical Transactions,* Vol. 21A, pp. 1527-1539, June 1990.

20. Barrettt, C.R., Nix, W.D., and Tetelman, A.S., *The Principles of Engineering Materials,* Prentice-Hall, Inc., 1973.

21. Smallman, R.E., *Modern Physical Metallurgy,* 4th ed., Butterworth and Coy, Ltd., 1985.

22. Pickering, F.B., *The Spectrum of Microalloyed High Strength Low Alloy Steels,* Sheffield City Polytechnic, Pond Street, Sheffield, England, pp. 1-27.

23. Bhadeshia, H.K.D.H., and Christian, J.W., "Bainite in Steels," *Metallurgical Transactions,* Vol. 21A, pp. 767-797, April 1990.

24. Korchynsky, M., "Microalloying and Thermo-Mechanical Treatment," *Processing, Microstructure, and Properties of HSLA Steels*, Deardo, A.J., ed., The Minerals, Metals and Materials Society, pp. 169-203, 1988.

25. Cohen, M., and Hansen, S.S., "On the Fundamentals of HSLA Steels, HSLA Steels: Metallurgy and Applications," *Proceedings,* International Conference on HSLA Steels, ASM International, pp. 61-71, 1985.

26. Speer, J.G., and Hansen, S.S., "Austenite Recrystallization and Carbonitride Precipitation in Niobium Microalloyed Steels," *Metallurgical Transactions A,* Vol 20A, pp. 25-38, January 1989.

27. Kiesling, R., and Lange, N., *Non-Metallic Inclusions in Steel, Parts I-IV*, The Metal Society, London, 1978.

28. Sanbongi, K., "Controlling Sulfide Shape with Rare Earths or Calcium During Processing of Molten Steel," *Transaction of ISIJ,* Vol. 19, pp. 1-9, 1979.

29. Kiesling, R.K., *Non-Metallic Inclusions in Steel, Part V,* The Institute of Metals, London, 1978.

30. Mikalac, S., (DTRC Code 2814) Letter to Lt Thomas C. Mohr, Subject: Chemical Composition and Processing of HSLA-100 with Increased Copper Steel.

31. Wilson, A.D., "Characterizing Inclusion Shape Control in Low Sulfur C-Mn-Cb Steels, HSLA Steels," *Proceedings,* Technology and Applications Conference, Philadelphia, Pennsylvania, ASM, pp. 419-427, October 1983.

32. Howell, P.R., and Varughese, R., "Austenite Transformation Products in Quenched Low-Carbon HSLA Steel," *Proceedings,* XXII International Congress for Electron Microscopy, San Francisco, California, pp. 902-903, 1990.

33. Dahmen, U., Ferguson, P., and Westmacott, K.H., "Invariant Line Strain and Needle-Precipitate Growth Directions in Fe-Cu," *Acta Mellurgica,* Vol. 32, no. 5, pp. 803-810, 1984.

INITIAL DISTRIBUTION LIST

		No. Copies
1.	Defense Technical Information Center Cameron Station Alexandria, Virginia 22304-6145	2
2.	Library, Code 52 Naval Postgraduate School Monterey, California 93943-5002	2
3.	Department Chairman, Code ME/Hy Department of Mechanical Engineering Naval Postgraduate School Monterey, California 93943-5000	1
4.	Naval Engineering Curricular Office, Code 34 Naval Postgraduate School Monterey, California 93943-5000	1
5.	Professor A.G. Fox, Code ME/Fx Department of Mechanical Engineering Naval Postgraduate School Monterey, California 93943-5000	2
6.	Dr. M.G. Vassilaros, Code 2814 David Taylor Research Center Annapolis, Maryland 21402	1
7.	Ms. Stephanie Mikalac, Code 12814 David Taylor Research Center Annapolis, Maryland 21402	1
8.	LT Thomas C. Mohr, USN 1511 41st Avenue San Francisco, California 94122	3